

**DIGITAL HYDRAULICS IN ELECTRIC HYBRID VEHICLES TO
IMPROVE EFFICIENCY AND BATTERY USE**

by

Jorge A. Leon-Quiroga

A Dissertation

Submitted to the Faculty of Purdue University

In Partial Fulfillment of the Requirements for the degree of

Doctor of Philosophy



School of Engineering Technology

West Lafayette, Indiana

August 2020

**THE PURDUE UNIVERSITY GRADUATE SCHOOL
STATEMENT OF COMMITTEE APPROVAL**

Dr. Jose Garcia, Chair

School of Engineering Technology

Purdue University

Dr. Brittany Newell

School of Engineering Technology

Purdue University

Dr. Jason Ostanek

School of Engineering Technology

Purdue University

Dr. Andres Gonzalez

School of Mechanical Engineering

University of the Andes, Colombia

Approved by:

Dr. Kathryne A. Newton

*Dedicated to my family, my friends, and all the people that supported me during this process.
Thanks for these amazing years and all the wonderful experiences that I will never forget. I will
have them in my heart forever.*

TABLE OF CONTENTS

TABLE OF CONTENTS.....	3
LIST OF FIGURES	6
ABSTRACT.....	9
CHAPTER 1. INTRODUCTION	10
1.1 Statement of the problem.....	10
1.2 Scope.....	12
1.3 Significance.....	12
1.4 Objectives	13
1.5 Assumptions.....	13
1.6 Limitations	14
1.7 Definitions.....	15
CHAPTER 2. REVIEW OF LITERATURE	16
CHAPTER 3. METHODOLOGY.....	26
3.1 Description of the system.....	26
3.2 Description of the test bench.....	28
3.3 Experimental tests.....	30
3.4 Numerical simulations	30
CHAPTER 4. EFFICIENCY COMPARISON	32
4.1 Energy tests for a hydraulic accumulator.....	32
4.2 Energy tests for an arrangement of ultracapacitors.....	36
4.3 Results for the hydraulic accumulator	39
4.4 Results for the ultracapacitors.....	39
4.5 Comparative results	40
CHAPTER 5. NUMERICAL MODEL OF THE TESTBENCH.....	42
5.1 Prime mover model.....	42
5.2 Hydraulic system modeling	46

5.3 Load simulator model	50
CHAPTER 6. TESTBENCH IMPLEMENTATION.....	53
6.1 General description	53
6.2 Prime mover.....	54
6.3 Hydraulic system	56
6.4 Load simulator	58
6.5 Instrumentation	59
6.5.1 Accelerator Input	59
6.5.2 Speed Controller	62
6.5.3 Pressure Controller	64
6.5.4 Data Acquisition System	65
6.6 Control algorithm.....	67
6.6.1 Speed Control	67
6.6.2 Pressure Control.....	68
CHAPTER 7. RESULTS	70
7.1 Numerical Model Results	70
7.2 Testbench Results	73
CHAPTER 8. CONCLUSIONS AND FUTURE WORK	79
REFERENCES	82

LIST OF FIGURES

Figure 1.1 Hydraulic system used for energy regeneration in electric vehicles (Leon Quiroga et al., 2017).	10
Figure 1.2. Hydraulic system with a three-way flow control valve.....	11
Figure 1.3. Digital hydraulics system.	11
Figure 2.1. U.S. Energy consumption by source and sector in 2018 (<i>U.S. Energy Information Administration (EIA) - Total Energy Monthly Data</i> , n.d.).....	16
Figure 2.2. Base demonstration vehicle in the study of Sprengel et al., 2015.....	19
Figure 2.3. Demonstration vehicle CAD render (Sprengel et al., 2015).	19
Figure 2.4. Demonstration vehicle underbody (Sprengel et al., 2015).	19
Figure 2.5. Hybrid hydraulic powertrain used in the study of Bender et al, 2014.....	20
Figure 2.6 Network of valves used in an excavator (Andruch & Lumkes, 2009).	22
Figure 3.1. Schematic representation of the hydraulic system.	26
Figure 3.2. Hydraulic system while is charging the accumulator.....	27
Figure 3.3. Hydraulic system while is using the energy from the accumulator.....	27
Figure 3.4. Schematic representation of the test bench.	28
Figure 3.5. Schematic representation of the test bench during operation as a hydrostatic transmission.	29
Figure 3.6. Schematic representation of the simulation and the vehicle.	31
Figure 4.1. Hydraulic accumulator.	32
Figure 4.2. Ultracapacitor.	32
Figure 4.3. Schematic representation for the hydraulic accumulator test bench.	33
Figure 4.4. Hydraulic test bench during charging mode.....	33
Figure 4.5. Hydraulic test bench during discharging mode.	34
Figure 4.6. Pressure in the accumulator during the charging and discharging process.	35
Figure 4.7. Pressure (top) and flow rate (bottom) while charging.....	35
Figure 4.8. Pressure and flow rate while discharging.	36
Figure 4.9. Schematic representation of the test bench for ultracapacitors.	36
Figure 4.11. Radar plot comparing three energy storage systems.	40
Figure 4.12. Radar plot comparing ultracapacitors and hydraulic accumulators.	41

Figure 5.1. Driving circuit for the permanent magnet ac motor	42
Figure 5.2. Switching signals for the logical gates	43
Figure 5.3. Simulink model of the inverter.....	44
Figure 5.4. Simulink model of the electric motor	45
Figure 5.5. Subsystem “AC_Machine model”	45
Figure 5.6. Hydraulic system model	49
Figure 5.7. Schematic representation of the load simulator.....	50
Figure 5.8. Control algorithm model for the electric generator.....	52
Figure 6.1. Subsystems in the testbench	53
Figure 6.2. Schematic representation of the prime mover of the testbench.....	54
Figure 6.3. LiFePO4 Battery pack used in the testbench.....	55
Figure 6.4. Inverter used in the testbench	55
Figure 6.5. Circuit design schematic and connection to Raspberry Pi 4.	56
Figure 6.6. Schematic representation of the hydraulic system	57
Figure 6.7. Schematic representation of the load simulator.....	58
Figure 6.8. Load simulator of the testbench	59
Figure 6.9. Original control box.	60
Figure 6.10. Digital control box used in the testbench.	61
Figure 6.11. Schematic representation of the control loop for the speed in the hydraulic motor.	62
Figure 6.12. Circuit prototype used for the flow rate measurement in the Raspberry Pi 4.	63
Figure 6.13. Schematic representation of the pressure controller hardware.	64
Figure 6.14. Devices used in the hardware of the pressure controller	65
Figure 6.15. Complete control algorithm diagram.....	67
Figure 6.16. Schematic representation of the control algorithm in the speed control	68
Figure 6.17. Schematic representation of the control algorithm for the pressure control system	69
Figure 7.1. Simulation results for the inverter	70
Figure 7.2. Pressure in the accumulator for different operating conditions.....	71
Figure 7.3. Power in the hydraulic pump for different operating conditions.	71
Figure 7.4. Current for the battery.	72
Figure 7.5. Pressure results comparison.	72
Figure 7.6. Control signal for the electric generator.....	73

Figure 7.7. Hydraulic variables in the system as the load changes.....	73
Figure 7.8. Hydraulic variables in the system as the load changes with one or six rheostats.	74
Figure 7.9. Power in the system and efficiency.	74
Figure 7.10. Power in the system and efficiency as the load changes with one or six rheostats..	75
Figure 7.11. Angular speed and pressure in the system.....	75
Figure 7.12. Pressure, shaft speed, and control signals in the hydraulic testbench.	76
Figure 7.13. Actual speed and reference speed comparison.	76
Figure 7.14. Flow rate in the system for different tests.	77
Figure 7.15. Flow rate test for a variable input reference.	77

ABSTRACT

The transportation sector consumes around 70% of all petroleum in the US. In recent years, there have been improvements in the efficiency of the vehicles, and hybrid techniques that have been used to improve efficiency for conventional combustion vehicles. Hydraulic systems have been used as an alternative to conventional electric regenerative systems with good results. It has been proven that hydraulic systems can improve energy consumption in conventional combustion vehicles and in refuse collection vehicles. The control strategy has a large impact on the performance of the system and studies have shown the control strategy selection should be optimized and selected based on application. The performance of a hydraulic accumulator was compared with the performance of a set of ultracapacitors with the same energy storage capacity. The energy efficiency for the ultracapacitor was around 79% and the energy efficiency of the hydraulic accumulator was 87.7%. The power/mass ratio in the set of ultracapacitors was 2.21 kW/kg and 2.69 kW/kg in the hydraulic accumulator. The cost/power ratio is 217 US\$/kW in the ultracapacitors and 75 US\$/kW in the hydraulic accumulator. Based on these results, the hydraulic accumulator was selected as the energy storage device for the system. A testbench was designed, modeled, implemented to test the energy storage system in different conditions of operation. The experimental results of the testbench show how the system can be actively controlled for different operating conditions. The operating conditions in the system can be adjusted by changing the number of rheostats connected to the electric generator. Different variables in the system were measured such as the angular shaft speed in the hydraulic pump, the torque and speed in the hydraulic motor, the pressure in the system, the flow rate, and the current and voltage in the electric generator. The control algorithm was successfully implemented, the results for the pressure in the system and the angular speed in the electric generator show how the control system can follow a desired reference value. Two different controllers were implemented: one controller for the pressure in the system, and one controller for the speed.

CHAPTER 1. INTRODUCTION

1.1 Statement of the problem

Hydraulic devices have been used as a method for energy recovery for braking in prototype hybrid combustion engine vehicles with similar results when compared with their electric counterparts (M. Ivantysynova & M. Sprengel, 2013) (Sprengel et al., 2015). These previous studies demonstrate the convenience of using hydraulic devices in hybrid vehicle applications. For the hydraulic devices, it is necessary to have a control variable to adjust the torque and the angular velocity because those devices are connected to the wheels, so the dynamics of the vehicle and the dynamics of the hydraulic system are coupled. In conventional hydraulic systems, the control variables are the displacement of the hydraulic pump and the displacement of the hydraulic motor (Figure 1.1) (Leon Quiroga et al., 2017), but the efficiency of the system is reduced dramatically when the displacement of the hydraulic devices change to have different transmission ratios.

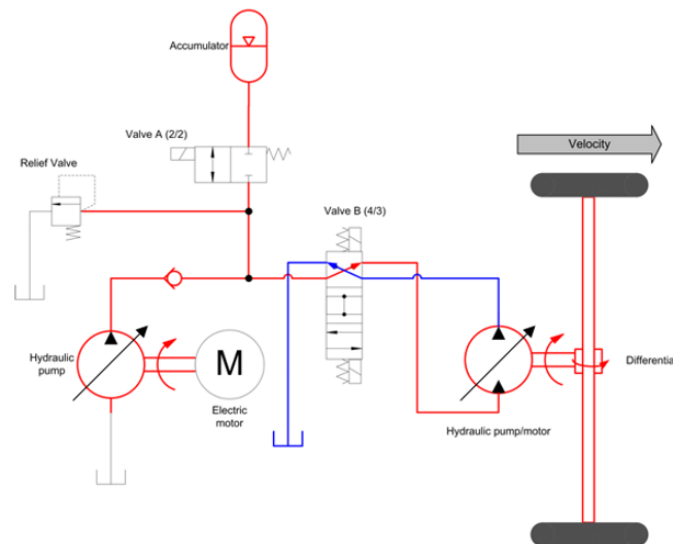


Figure 1.1 Hydraulic system used for energy regeneration in electric vehicles (Leon Quiroga et al., 2017).

Another option to control the flow and pressure in a hydraulic system involves the use of a flow control valve, but the problem with this kind of valve is that the energy losses are considerably large. An example system is shown in figure 1.2. These systems (figure 1.2) use relief valves and

orifices to regulate the flow and the pressure for the final user. The desired flow rate is Q_f and the final pressure that is going to the user is p_f . The excess of flow is sent to the tank through the relief valve, and the excess in pressure is lost through the orifice.

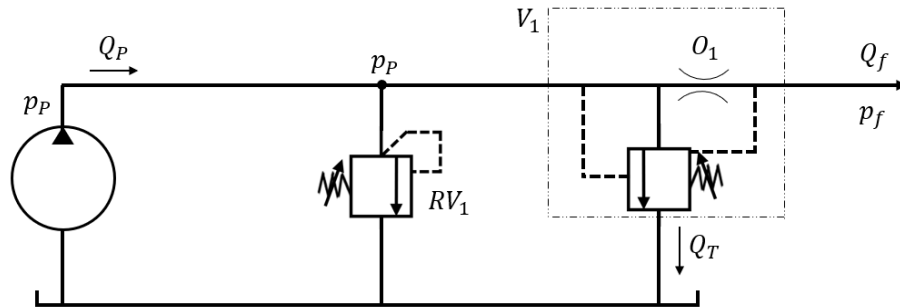


Figure 1.2. Hydraulic system with a three-way flow control valve.

An alternative unconventional option includes an arrangement of accumulators connected in series. The flow can be controlled by allowing the flow through the accumulators with 2 position directional control valves. The pressure of the system, which is related to the torque, is a function of the number of active accumulators. Therefore, the number of active accumulators can be used as a control variable. A schematic representation of this system is shown in figure 1.3.

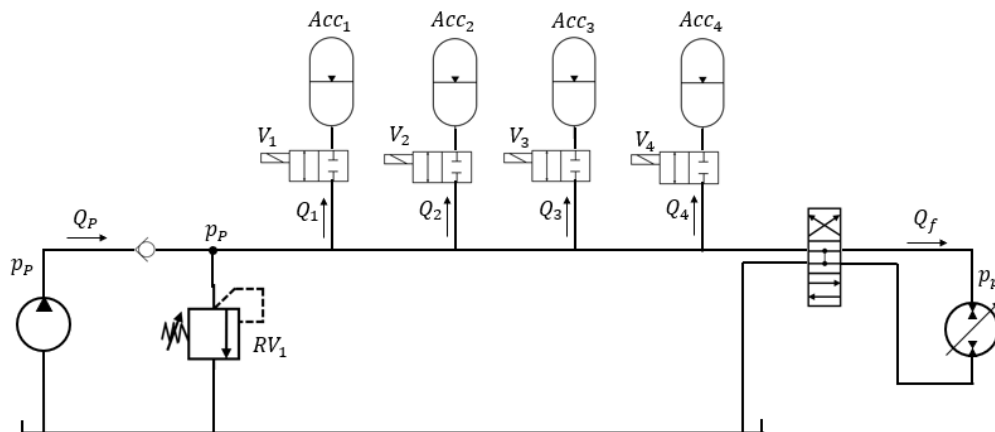


Figure 1.3. Digital hydraulics system.

The approach of using non-proportional valves for flow modulation is known as digital hydraulics. This approach does not throttle the flow like control orifices and is known to be more efficient

(Merrill et al., 2010). The purpose of this work is to compare the performance of a hydraulic accumulator and a set of ultracapacitors, and then design and model a testbench with an energy storage system selected according to the results obtained. This testbench could be used in the future to test a digital a hydraulic system.

1.2 Scope

The scope of this work focuses on the construction of a testbench for simulating a hydraulic system operating following the driving schedules for a heavy-duty cycle vehicle such as an urban bus. The control strategy for the system is going to be incorporated into the test-bench. For the test bench, the scope will be to measure the performance of the hydraulic system for specific combinations of number of valves and hydraulic pump velocities. In addition to the test-bench, a complete model for the hydraulic system fitted to the transmission of an electric bus will be made. The simulation will take, as an input, a driving schedule and the output will be the performance variables of the vehicle such as the energy consumption, torque at the electric motor, the State of Charge (SOC) of the battery, the pressure in the hydraulic system, and the SOC of the hydraulic accumulators. A simulation of the system will also be developed in Matlab/Simulink and validated using experimental results. A comparison between a hydraulic accumulator and a set of ultracapacitors will be made.

1.3 Significance

This is a multidisciplinary research project incorporating application of vehicle dynamics, fluid power, hybrid systems, and control systems. This project expands the knowledge in the field of vehicle dynamics because the purpose is to study a new non-conventional vehicle architecture and develop models and experiments to understand the dynamics of the vehicle providing design tools to future engineers and technologists. In the field of fluid power, the contribution will be a new tool to simulate experimentally and numerically different operating conditions of load and input for electro-hydraulic applications. The contribution in the field of hybrid systems will be the use of an energy storage system as an alternative source of power for an electric vehicle. One of the benefits of this system is the possibility of controlling the different operating conditions from the

input power and the input dynamics, the hydraulic variables such as the pressure and the flow rate, and the dynamic, electrical, and power outputs in the load simulator. In the field of control systems, the contribution will be the construction of a tool that can be used to test any control algorithm experimentally, and a mathematical model of the system that can be used as a design tool for electro-hydraulic applications.

1.4 Objectives

The research question that will be answered in this project is: is the performance of a hydraulic accumulator better than the performance of a set of ultracapacitors if both systems are tested under similar conditions of operation?

Based on the statement of the problem, the scope and the significance, the following general objective is proposed:

Develop an experimental and a numerical tool to study the performance of an electro-hydraulic system with energy regeneration.

The following specific objectives are proposed:

- Compare the performance characteristics of a hydraulic accumulator and a set of ultracapacitors under similar conditions of operation.
- Design and build a testbench to evaluate a hydraulic regenerative system under different conditions of operation.
- Develop a numerical model of the proposed testbench to develop the controllers to be used in the testbench.

1.5 Assumptions

The assumptions are going to be made for two parts of the work: the simulation part and the experimental part. The assumptions are related to the driving schedule, the parameters of the vehicle, the parameters of the electric devices and the parameters of the hydraulic devices.

The assumptions for the experimental part of this study are listed below:

1. The dynamics of the test bench works comparably to the dynamics of a vehicle.
2. The driver is assumed as ideal, so the driver can follow all the changes in the driving schedule.

The assumptions for the simulation part of this study are listed below

1. There is no slip in the tires of the vehicle.
2. The loads over the vehicle's tires are assumed as contact forces.
3. The vertical and lateral dynamics of the vehicle are not considered.
4. The mass of the vehicle is constant.
5. The flow rate out of the pump is the same as the flow rate entering into the hydraulic motor.

1.6 Limitations

The limitations for the simulation part of this study are listed next:

1. The simulation is not able to determine the energy losses through heating of the components.
2. The model cannot make estimations of emissions in the vehicle.

The experimental part has some limitations as well:

1. The test bench is not able to replicate sudden changes made by an actual bus driver.
2. It is not possible to estimate the drivability with the test bench.
3. The data collected is sensitive to the instruments used and their calibration.
4. Since the data is going to be collected on a test bench, there is the possibility that the data collected in an actual bus could be different.

1.7 Definitions

This section presents some important definitions that are useful to understand the concepts related with this project.

Digital hydraulics: in digital hydraulic systems, the proportional valves are replaced by many on/off valves that are turned on and off to change the flow rate in the system (Andruch & Lumkes, 2009).

Driving schedule: a driving schedule is a plot of velocity vs time for a vehicle (Boretti, 2017). There are some commonly used driving schedules such as the New European Driving Schedule and the EPA Urban Dynamometer Driving Schedule (US EPA, 2015).

State of charge (SOC): the state of charge is the ratio between the actual amount of energy in the system and the maximum energy storage capacity. The value of the state of charge is between 0 and 1 (M. Ivantysynova & M. Sprengel, 2013).

Hydraulic accumulator: in a hydraulic accumulator the energy can be saved with a pressurized fluid. Accumulators can be used as energy storage devices in regenerative braking energy systems (Sprengel et al., 2015).

CHAPTER 2. REVIEW OF LITERATURE

Oil reserves are continually diminishing while the worldwide demand of energy continues to increase creating a supply and demand problem. Efforts have been made to reduce energy usage and there are many alternatives for supplying energy such as renewable energy, nuclear energy, biofuel energy, etc. For vehicles, gas emissions represent an additional problem due to their negative impact on the environment. Another option for reducing the impact of gas emissions is improving the efficiency of the systems and devices that are already in use. Any improvement in the efficiency of devices can be significant and can have a global impact. Current energy consumption by sector is presented in figure 2.1. This information was taken from the website of the U.S. Energy Information Administration (*U.S. Energy Information Administration (EIA) - Total Energy Monthly Data*, n.d.).

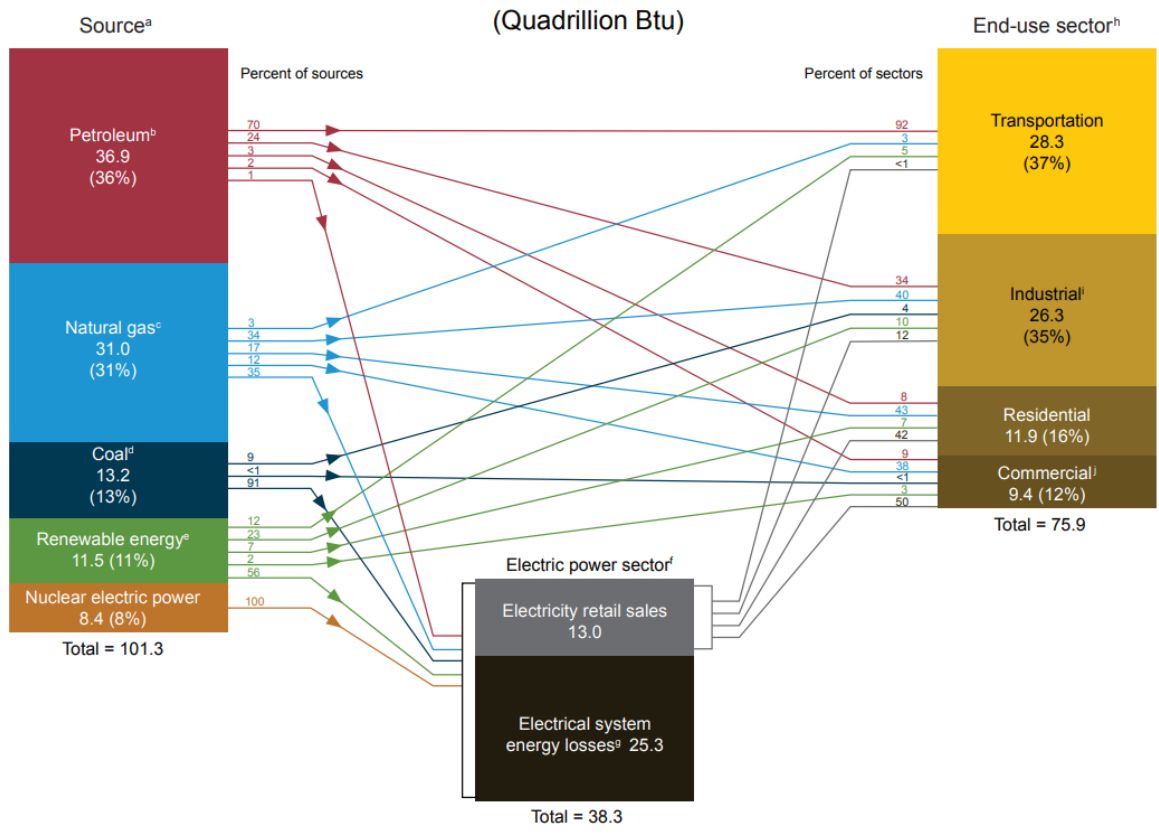


Figure 2.1. U.S. Energy consumption by source and sector in 2018 (*U.S. Energy Information Administration (EIA) - Total Energy Monthly Data*, n.d.).

According to the U.S. Energy Information Administration, in 2018 in the United States the transportation sector consumed 70% of all petroleum-based energy. So, improving the efficiency of the transportation systems can have a huge impact on the global energy consumption.

Due to recent concern about reducing emissions in traditional combustion engine vehicles, electric vehicles have been considered as an alternative for replacing traditional vehicles. Electric vehicles use an electric motor as the prime mover and flywheels, fuel cells, ultracapacitors and batteries as energy sources (Ahmadkhanlou & Goodarzi, 2011; Beaman & Rao, 1998; Cao & Emadi, 2012; Hu, 2012; Ju et al., 2014; Lukic et al., 2008). The advantages of electric vehicles over internal combustion engine vehicles are the high efficiency, smooth and quiet operation, no emissions and independence from petroleum based fuels (Ehsani, 2018).

Despite the advantages of electric and hybrid vehicles, there has been a slow adoption of this technology around the world. The principal concern about electric and hybrid vehicles is its driving range. Even though there is a huge concern about low driving range in electric vehicles, it has been demonstrated that, in general, people demand more driving range than they actually need (Franke et al., 2012). The results of the study made by Thomas Franke and Josef Krems (Franke & Krems, 2013) show that the actual driven distances are lower than the expected driving range. In the study of Pearre et al (Pearre et al., 2011) it was demonstrated that the mean daily driving distance for light-duty vehicles is 45 miles. In the same study, it was found that on average just for nine days of the year, people drive more than 150 miles. These studies demonstrate that there is an overestimation of driving range in vehicles. Also, if the driving range of EV is around 150 miles, it is possible to satisfy the average requirements of the light-duty vehicle users except for nine days a year.

There have been some studies regarding driving range of heavy-duty vehicles (N. Clark et al., 2007). School bus drive cycles were collected in a study conducted by Duran and Walkowicz (Duran & Walkowicz, 2013). The study includes data from 1500 individual route shifts for Washington, New York, and Colorado. The results of the study show that the average daily distance covered by the school buses is around 73.46 miles, the 99.7% confidence interval of the

study was found to be from zero to 154.46 miles per day. These results are very important to identify the potential for electrification and hybridization for this kind of vehicle type. Table 1 shows a comparison between the current driving range for electric buses used in school transportation. The information in table 1 shows that the current technology in electric school buses is close to satisfying the driving range found in the study mentioned above.

Table 1. Comparison of current driving range in electric school buses

Manufacturer	Battery Capacity	Driving Range	Charging Time
The Lion Electric Co.	176 kWh	125 miles	6 - 7 hours
Blue Bird	160 kWh	120 miles	6 - 8 hours
Starcraft eQuest XL	127 kWh	100 miles	8 hours
BYD C6M	121 kWh	95 miles	3 – 4 hours

Despite the studies made regarding driving range, drivers concern and perception of the range issue is an obstacle for electric vehicles and hybrids to overcome in order to become a popular alternative (Egbue & Long, 2012; Laser & Lynd, 2014; Rezvani et al., 2015; Wager et al., 2014). Because of this reason, it is necessary to find alternatives to improve the efficiency of the vehicles, extend battery life, extend driving range, and reduce maintenance cost to make them more attractive to customers.

Powertrain hybridization through hydraulic transmission is one of the available options for improving efficiency in electric and conventional cars (Bozic, 2007; Buchwald et al., 1979; Sun Hui et al., 2010; M. Ivantysynova & M. Sprengel, 2013; Riviera, 1983; J. Zhang et al., 2012; Zhuge & Kazerani, 2014). The on-road hybrid vehicle market is dominated by electric hybrids, however hydraulic hybrids have many benefits which make them a competing technology. It has been demonstrated that hydraulic hybrid transmissions increase the fuel efficiency by 29% compared to the most efficient electric hybrid and 47% over an identical non-hybrid bus (Mike Heskitt et al., 2016). Moreover, the lifecycle cost of the hydraulic hybrid is 24% less than a conventional diesel bus and 36% less than an electric hybrid bus (Bender et al., 2014; B. Wu et al., 2004). Hydraulic hybrids use hydraulic accumulators as energy storage devices. Accumulators have a longer lifecycle than batteries and the batteries need to be replaced one or more times over their lifetime

depending on application (Chrostowski & Kędzia, 2005; N. Clark et al., 2007). An example of the use of hydraulic systems for conventional vehicles is shown in figure 2.2, figure 2.3 and figure 2.4 (Sprenzel et al., 2015).



Figure 2.2. Base demonstration vehicle in the study of Sprenzel et al., 2015.

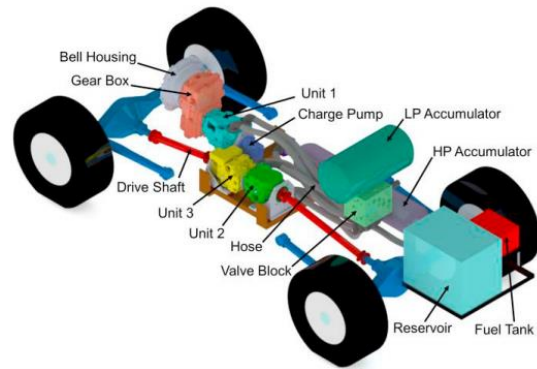


Figure 2.3. Demonstration vehicle CAD render (Sprenzel et al., 2015).

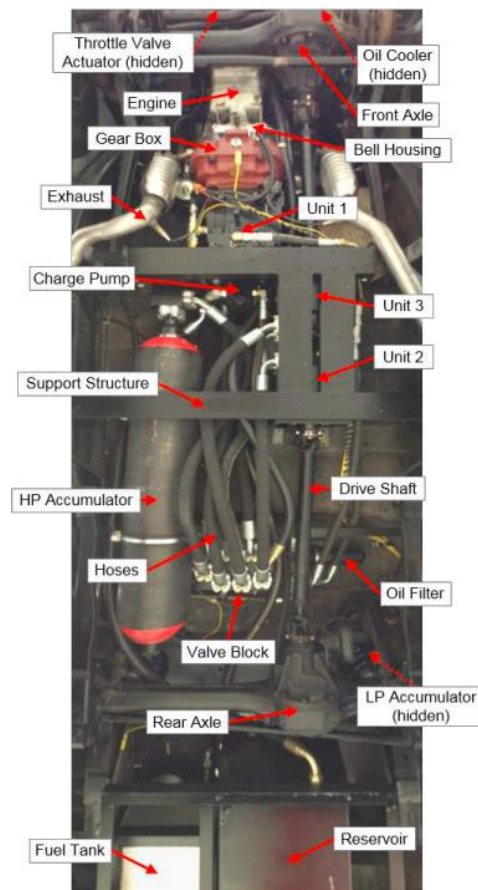


Figure 2.4. Demonstration vehicle underbody (Sprenzel et al., 2015).

Hydraulic systems have demonstrated their convenience as regenerative systems (K.-E. Rydberg, 2009; Kepner, 2002; Liu et al., 2009). The dynamics of the vehicle are considerably affected, and it is necessary to choose the correct application for hydraulic systems. One example of a good application of hydraulic systems can be found on refuse collection vehicles (Bender et al., 2014) and delivery trucks (B. Wu et al., 2004). The fuel savings in this kind of vehicles depends on the driving schedule. It is necessary to have a driving schedule with many braking events because the kinetic energy of the vehicle from this motion can be saved in the hydraulic accumulators. The study of Bender et al. shows that the energy saving is around 20% with respect to a vehicle without a hydraulic system. This result is important because it shows that this kind of system can be used in vehicles with similar characteristics such as commercial passenger buses. The hydraulic system used in this study is connected in parallel with the combustion engine. A schematic representation of the system is shown in figure 2.5.

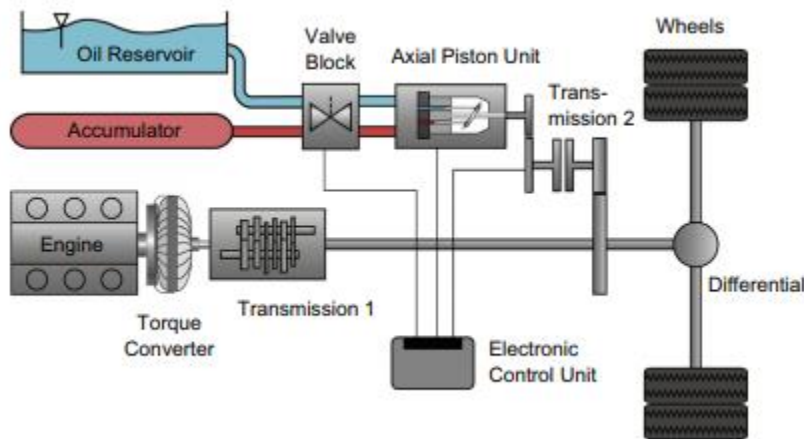


Figure 2.5. Hybrid hydraulic powertrain used in the study of Bender et al, 2014.

There are some additional advantages in hydraulic systems. Hydraulic systems have higher power density than electric systems which are usually used in regenerative systems in vehicles (Liu et al., 2009). It has been proven that hydraulic regenerative systems can be used for conventional vehicles, such as sport utility vehicles, with good results (Sprenkel et al., 2015). The hydraulic regenerative system can be used in parallel with the conventional combustion engine. The control strategy of the system is very important, and in this study, the authors have proposed a control strategy based

on the position of the throttle and brake pedals. This study presents a detailed explanation of the hydraulic system used and the experiments made to measure the principal variables of performance in the vehicle.

The control strategy has a crucial role in vehicle performance (Baumann et al., 2000; Itani et al., 2016; Rajagopalan et al., 2003; X. Zhang & Mi, 2011), and in a hydraulic system (Jing et al., 2018). Fuzzy logic control has been proposed as a control strategy for parallel hybrid electric vehicles because it can be used to optimize the dynamic characteristics of the vehicle without increasing the energy consumption (Matheson & Stecki, 2003; C. Wang et al., 2011). Fuzzy logic is a non-conventional control strategy for vehicle powertrain (Baumann, 1997; Hyeoun-Dong Lee et al., 2000; Jalil & Kheir, 1998; Kono, 1998; Njabeleke et al., 1998; Schouten et al., 2002; C. Wang et al., 2011) but it is worthwhile to test its convenience. The research team of the Adaptive Additive Technologies Lab at Purdue University studied fuzzy logic as a control strategy for a commercial bus in Bogotá, Colombia (Leon Quiroga et al., 2017). The results show the utility of this control strategy for this vehicle type. The results obtained using fuzzy logic control were similar to the results obtained when a conventional control strategy, such as PID control, was used.

The control strategy for a hydraulic hybrid vehicle must be able to adjust the pressure and the flow rate in the system. Hydraulic regenerative systems use conventional hydraulics that use variable displacement units to adjust velocity and torque according to the requirements of the vehicle and its driving schedule (Bleazard et al., 2015; Sprengel & Ivantysynova, 2014). The efficiency in these systems is strongly affected by the displacement of the hydraulic units. Another way to control torque and velocity in hydraulic systems is through digital hydraulics. In digital hydraulics the flow is controlled using valves which are either turned on or off according to the requirements of the user. Some digital hydraulic systems have been proven effective and simulated with good results (Andruch & Lumkes, 2009; Holland, 2012; Merrill et al., 2010; Pavel et al., 2017). The efficiency in this system is better compared with conventional hydraulic systems and digital hydraulics can be used in applications such as hydraulic excavators and regenerative braking systems. An example of the use of digital hydraulics in an excavator is shown in figure 2.6 (Andruch & Lumkes, 2009). In this example, the conventional orifices are changed by non-

proportional 2-way-2-position valves, which improves the efficiency of the system. With the valves used in this system it is possible to adjust the flow rate and the pressure in the actuators.

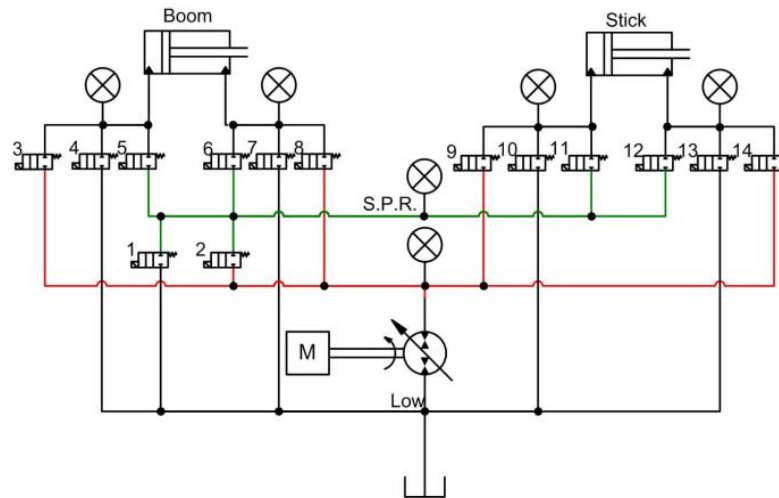


Figure 2.6 Network of valves used in an excavator (Andruch & Lumkes, 2009).

Some other alternatives to regenerate energy with hydraulic systems have been proposed (Andruch & Lumkes, 2009; Kwon et al., 2010; T. Lin et al., 2018; Tianliang Lin et al., 2010; B. Wang, 2014; T. Wang et al., n.d.; Xiao et al., 2018). An accumulator can be used to store fluid and energy in a conventional closed loop hydraulic system. This accumulator can be used to control the velocity in the system. It has been proved that the accumulator improves the efficiency in the system because the energy stored in it can be used later. In contrast, in a conventional system without an accumulator, the control of the velocity is made through a proportional valve in which the energy is lost as heat (Wiens & Bitner, 2016). The study of Wiens and Bitner is important because the authors present a new architecture for closed circuit linear actuators, this architecture can be extrapolated to other systems such as regenerative braking energy devices.

It is important to consider the electric systems that are already in use as regenerative systems. Some previous studies have been done to compare the different kinds of technology used in hybrid electric vehicles (Ehsani, 2018; Huria et al., 2012; Keil & Jossen, 2014; Liang et al., 2013; Tianliang Lin et al., 2016, 2017; Z. W. Wu et al., 2012). The configurations that have been used over the last years include the series configuration, the parallel configuration and a combination

of parallel and series configurations. The control techniques that have been used are focused on different goals such as maximum fuel economy, minimum emissions, minimum system cost and good driving performance (Çağatay Bayindir et al., 2011). The comparison made in this work is useful to see the advantage of the hybrid vehicles compared with the conventional combustion vehicles.

Ultracapacitors are the main competitor for hydraulic accumulators in energy regeneration applications (Cheng, 2010; Jiang et al., 2013; Miller & Mitchell, 2011; Minav et al., 2009; Nielson & Emadi, 2011; Niu et al., 2017; Ostadi & Kazerani, 2015). Ultracapacitor systems are preferred in some applications such as wind turbines in remote areas where high power density is required (Tan et al., 2017), some other applications such as reducing engine size on rubber wheeled gantry cranes (Kim & Sul, 2006), and in biomedical applications (Pandey et al., 2011). It is necessary to have good numerical models to compare and design possible configurations of ultracapacitors and hydraulic accumulators. The correct model depends on the specific application of the ultracapacitor arrangement. Some models have been used over the last years. Some of these models are based on experimental data and some of them are based just on theoretical approaches. A comparison between some classic models was made in the work of L. Shi and M. L. Crow (2008). The principal purpose of this study is to show the principal differences between the models and talk about some advantages and disadvantages (Shi & Crow, 2008). Some previous studies have been focused on the performance characteristics of electric accumulators (Allagui et al., 2016; Fouda et al., 2016; Freeborn, 2016; Hartley et al., 2015; Kumar et al., 2019; Yoo et al., 2008), and some other have been focused on hydraulic accumulators performance when they are used as the main energy storage system (S. Hui et al., 2011; Pourmovahed et al., 1988; F. Wang, 2011). This work is developed with the intention of comparing these two systems side by side.

The models for ultracapacitors can be complex and the computational cost of them could be high. If a high-fidelity model is needed, a different approach could be used. Waveform relaxation techniques were used in the work of S. Moayedi, F. Cingoz, and A. Davoudi to do high-fidelity models of ultracapacitors. In this work the simulation time was reduced considerably when compared with a traditional simulation (Moayedi et al., 2013). The results were compared with experimental data.

The simulation for the electric regenerative system needs to be coupled with the dynamics of the vehicle and the mechanical parts. In some studies the input of the system is the velocity given by a driving schedule (Bleazard et al., 2015), in these studies the dynamics of the system is solved according to that input. The variables of the vehicle such as torque, motor speed, the control variables, and energy consumption depend on the input velocity (Gillespie, 1992). Some models included information about charging stations and include geographic information to make the model more real (Alegre et al., 2017) and the driving cycle must be considered (Ou et al., 2011).

The models need to have experimental validation to confirm the results. Hybrid vehicles have been tested in past works and it has been proved that this type of vehicles could be useful to reduce energy consumption (Ossyra & Ivantysynova, 2004). Ultracapacitors have been tested in some studies for long-life robust applications with good results. The test procedures can be used and replicated for any other specific application (Murray & Hayes, 2015). The experimental results could be used as inputs for the numerical model and this can improve the results.

With this literature review, it is possible to observe the alternatives that have been used for hybridization in vehicles to improve energy efficiency. Hydraulic systems are one of those alternatives and they have the advantage of having more power density than a conventional electric system (Hewko & Weber, 1990; Paladini et al., 2007; Stienecker et al., 2006). The power density in a conventional ultracapacitor is around 1 kW/kg while in a hydraulic accumulator is around 10 kW/kg (Leon et al., 2016). In a conventional hydraulic system, the velocity and the torque are controlled with the displacement of the hydraulic devices, the problem with this approach is that the efficiency is strongly dependent on the displacement. Another alternative is using an arrangement of valves or accumulators to control the flow rate, with this approach the hydraulic devices could work with a constant displacement which improves the efficiency of the system. This approach is called digital hydraulics. Digital hydraulics has been used successfully to control velocity of hydraulic actuators which can be used in hydraulic arms.

The principal competitor for the hydraulic system is an arrangement of ultracapacitors. Ultracapacitors are the electric equivalent to a hydraulic accumulator, but ultracapacitors have

some advantages and drawbacks that were explored in some previous works, such as self-discharge rate which causes energy losses of 10% to 20% per day in ultracapacitors, and the gradual voltage loss output in ultracapacitors as a function of the charge. It is necessary to have good models for both systems (electric system with ultracapacitors and hydraulic system with hydraulic accumulator) to design and compare the results for different kinds of applications. The present work aims to compare the efficiency of hydraulics and ultracapacitors in a physically representative test bench, and design a numerical and experimental tool to study the performance of an electro-hydraulic system.

CHAPTER 3. METHODOLOGY

3.1 Description of the system

Before describing the methodology, it is necessary to explain in depth the proposed hydraulic system. In an actual hybrid electric vehicle, a bidirectional fixed displacement pump/motor is connected directly to the wheels of the vehicle, a directional control valve is connected to the pump/motor with the hydraulic accumulator. The hydraulic accumulator is activated with a 2-way-2-position valve, and a relief valve is controlling the maximum pressure in the system. A schematic representation of the system is shown in figure 3.1. In this study, an electrohydraulic system that simulates the performance of the wheel-hydraulic pump interaction is designed, constructed and mathematically modelled. The mathematical model includes just one accumulator attached to the hydraulic system, as presented in figure 3.2.

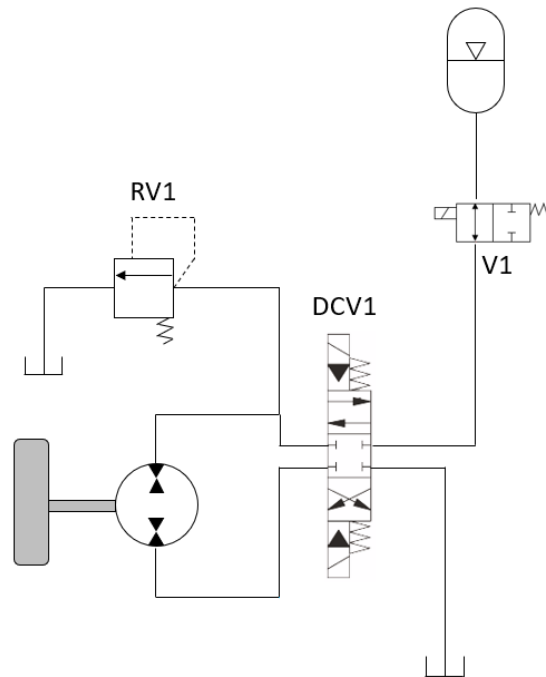


Figure 3.1. Schematic representation of the hydraulic system.

The hydraulic system can work in three different modes. The first mode is while braking, in this mode the hydraulic unit works as a pump which is moved by the kinetic energy of the vehicle (figure 3.2). The kinetic energy is stored in the accumulator as pressurized fluid. The second mode is when the energy stored in the accumulator is used to move the vehicle. In this mode the hydraulic unit is used as a motor which converts the hydraulic power from the accumulator to mechanical power to the wheels of the car (figure 3.3).

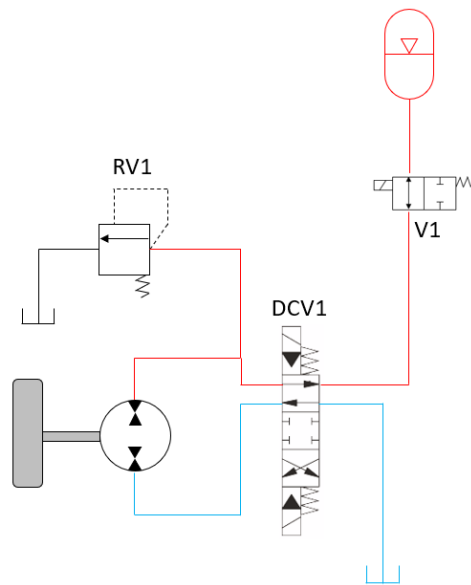


Figure 3.2. Hydraulic system while is charging the accumulator.

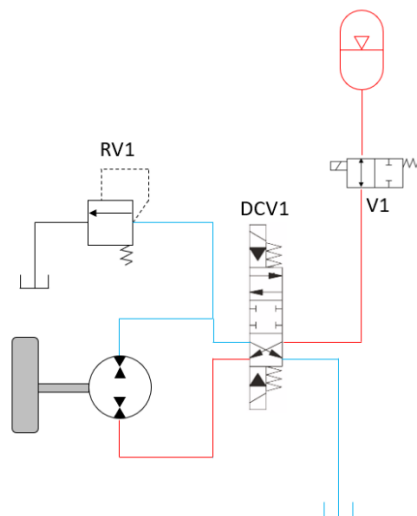


Figure 3.3. Hydraulic system while is using the energy from the accumulator.

In the actual system it is very important to control the flow rate and the pressure in the system to adjust the velocity and the torque in the wheels because this is going to affect the dynamic of the vehicle. The flow rate and the pressure are going to be controlled with an electric motor in the input and a load simulator in the output. A control system must be implemented for this purpose.

3.2 Description of the test bench

One of the purposes of this project is to create a test bench that can replicate the physical conditions of the real system in a vehicle. It is necessary to do the experimental tests in a similar way compared to the simulation approach. In the actual system in the vehicle, the hydraulic unit is moved with the kinetic energy of the vehicle, but in the test bench the wheel is going to be replaced by an electric motor. The electric motor is going to simulate the kinetic energy from the wheels during the propulsion mode. This electric motor is connected to a DC/AC converter, which is controlled with a Raspberry Pi 4. The versatility of the Raspberry Pi 4 is useful to simulate different conditions of operation for the testbench during propulsion mode, and braking mode. The schematic representation of the test bench is shown in figure 3.4.

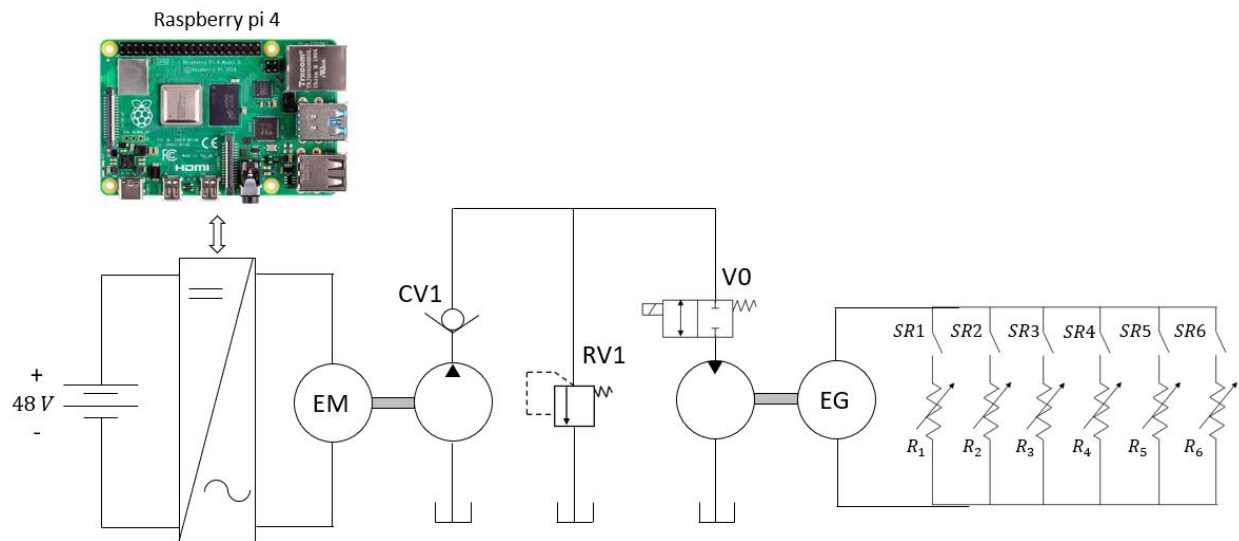


Figure 3.4. Schematic representation of the test bench.

The test bench can operate as a regular hydrostatic transmission while V0 is open. The load of the testbench is an electric generator that is attached to a set of rheostats. The load is adjusted with a PWM controller that is connected between the generator and the rheostats. The PWM signal is adjusted with the Raspberry Pi 4. The input speed of the testbench is adjusted with a PWM controller connected to the DC/AC converter and the signal is controlled with the Raspberry Pi 4. The schematic representation of the testbench for the operation as a hydrostatic transmission is presented in figure 3.5.

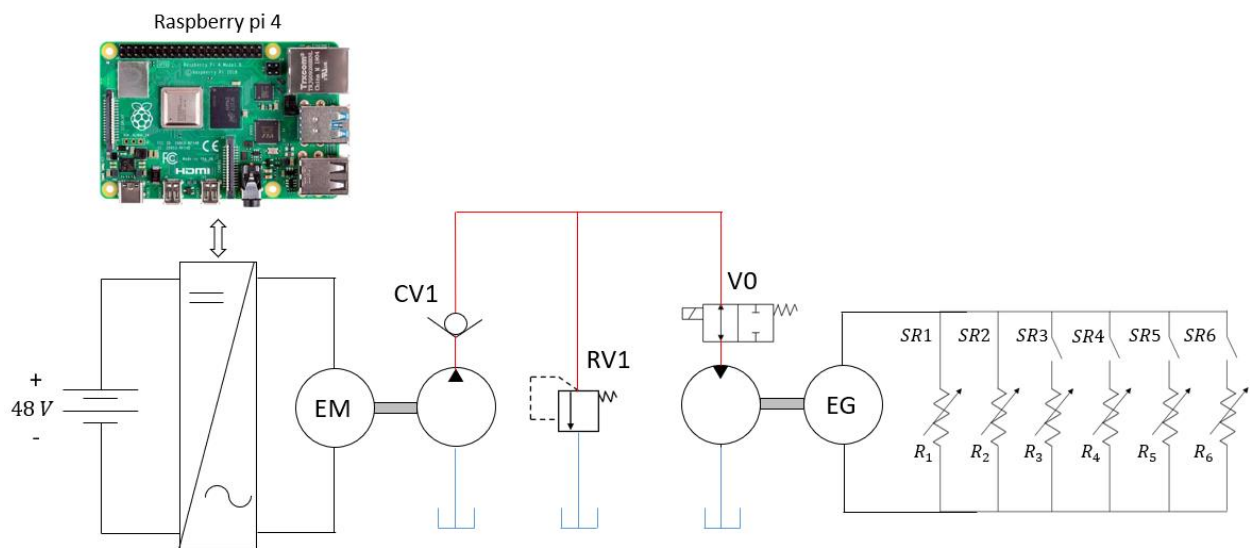


Figure 3.5. Schematic representation of the test bench during operation as a hydrostatic transmission.

The control strategy for the testbench is programmed with python using the Raspberry Pi 4. The control algorithm has either the desired pressure or the desired flow rate in the testbench as an input. The actual value for the pressure and the flow rate are measured through the time of operation of the testbench. The measured pressure and flow are compared with the desired value and the error is used to adjust the PWM signal used to control the electric current output in the electric generator to change the load and the pressure in the system. The flow rate is controlled by adjusting the PWM signal of the velocity controller of the electric motor that is used as the prime mover.

3.3 Experimental tests

It is necessary to measure the performance of the hydraulic system. In the hydraulic test bench, an electric motor is driving a hydraulic pump, and the hydraulic pump moves the flow to the hydraulic accumulators. The variables that can be measured in the hydraulic system are the pressure in the hydraulic pump output, the flow rate, the pressure in the accumulators, the voltage and current at the battery or the input power of the system, the angular speed in the electric motor, the angular speed in the electric generator, the voltage and current in the electric generator. With these variables it is possible to calculate the performance of the system. With this methodology it is possible to compare the hydraulic system using different operating conditions, and it is possible to calculate the efficiency for transmitting power in the testbench. The information regarding the sensors and instruments used in the testbench is presented in chapter 6 of this document.

3.4 Numerical simulations

The simulations will be made on Matlab/Simulink because of the advantages that this software can provide, including that Simulink has some useful libraries for simulations of vehicle dynamics, the interface is user friendly, and capable of representing the physical connections between the parts of the vehicle.

In these simulations the input will be the velocity of the vehicle from the driving schedule. After that, the pedal positions will be estimated with a driver model to make the simulations similar to real world conditions. The inputs for the driver model will be the desired velocity of the vehicle and the output will be the position of the braking and acceleration pedal. The general dynamics of the vehicle will be solved, the input for this part of the model will be the position of the pedals and the output will be the vehicle velocity and the torque in the wheels. The velocity calculated in this part of the simulation will be an input for the driver model. Now it is possible to solve the dynamics of the powertrain. The wheels are connected to the differential, and the differential is connected to the mechanical transmission, the mechanical transmission connects the prime mover (it could be either a combustion engine or an electric motor) with the differential and the wheels. From this simulation it is possible to calculate relevant variables of the vehicle such as torque at the wheels, torque at the prime mover, energy consumption, transmission efficiency. The description of the

simulations is valid for any kind of vehicle. A schematic representation of the vehicle and the simulation is shown in figure 3.5.

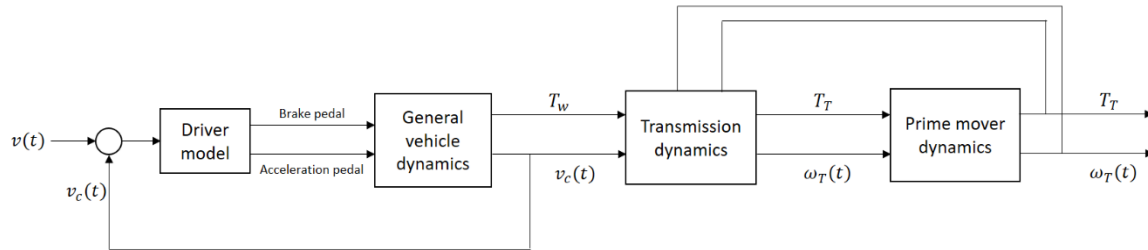


Figure 3.6. Schematic representation of the simulation and the vehicle.

The prime mover dynamics and the transmission dynamics can be modified according to the specifications of each application. These subsystems will be different for a hydraulic system and for the electric system, but the energy flow, the inputs and the output will be the same. The principal advantage of this simulation is the possibility to compare different systems with the same approach.

CHAPTER 4. EFFICIENCY COMPARISON

As a first step to answer the research questions formulated in this project, the efficiency of one single hydraulic accumulator is compared with the efficiency and performance of an arrangement of ultracapacitors. The main characteristics of the hydraulic accumulator and the ultracapacitor used are shown below in table 2:

Table 2. Characteristics of the hydraulic accumulator and the ultracapacitor used in this study

Hydraulic accumulator	
Manufacturer	Parker Hannifin
Reference	A2N0058D1K
Mass (lb)	10
Vol. Capacity(in3)	58
Max. Pressure (psi)	3000

Ultracapacitor	
Manufacturer	Maxwell Tech.
Reference	BCAP0050 P270 S01
Mass (g)	12.2
Energy Cap. (mWh)	50.6
Max. Voltage (V)	2.7
Max. Current (A)	6.1

The picture of a hydraulic accumulator and an ultracapacitor are shown in figure 4.1 and 4.2.



Figure 4.1. Hydraulic accumulator.



Figure 4.2. Ultracapacitor.

To compare both devices in a similar way, two test benches were designed and constructed. Both test benches are designed to measure charge and discharge variables of the systems.

4.1 Energy tests for a hydraulic accumulator

The schematic representation of the test bench designed and constructed for the hydraulic accumulator is presented in figure 4.3.

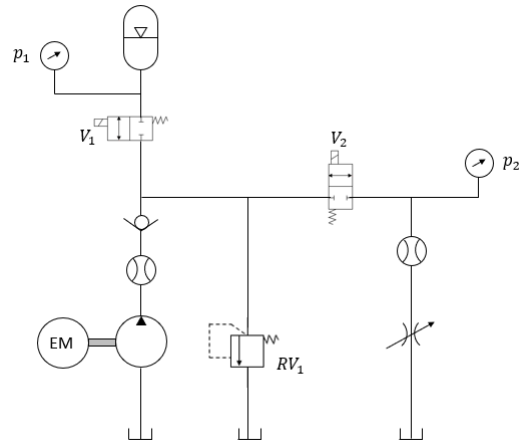


Figure 4.3. Schematic representation for the hydraulic accumulator test bench.

This test bench was designed to measure the flow of energy through the accumulator while charging and discharging. During charging mode, the electric motor is turned on and is used to move the hydraulic pump. The valve V1 is open, allowing the flow through the accumulator, while the valve V2 is close. The relief valve RV1 is close unless the relief pressure is reached. A schematic representation of the test bench during charging mode is presented in figure 4.4. The red lines show the high-pressure lines.

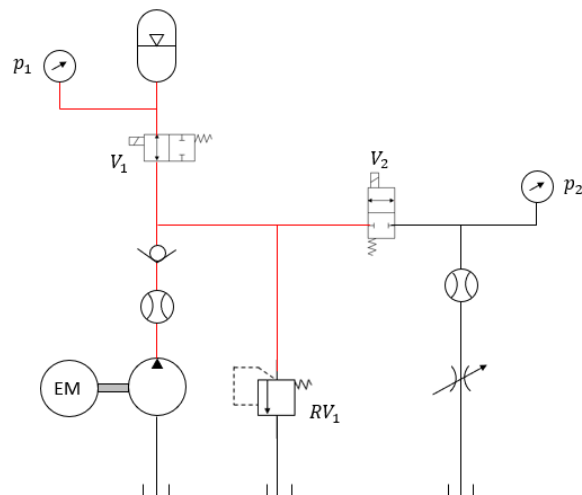


Figure 4.4. Hydraulic test bench during charging mode.

During the charging mode, the measured variables are the current and voltage in the battery connected to the electric motor, and the pressure and flow rate in the accumulator. With these

variables it is possible to calculate the power input from the battery, the power going to the accumulator, the consumption of electric energy, and the energy saved in the accumulator. The speed of the electric motor is adjusted with a controller, which is connected to the inverter.

A test for discharge was done to measure the efficiency of the hydraulic accumulator. In the discharge test, the output load was simulated with an orifice. The load applied to the hydraulic system increases when the valve is closed. A no-load condition is simulated if the valve is completely open. A schematic representation of the system during discharge mode is presented in figure 4.5.

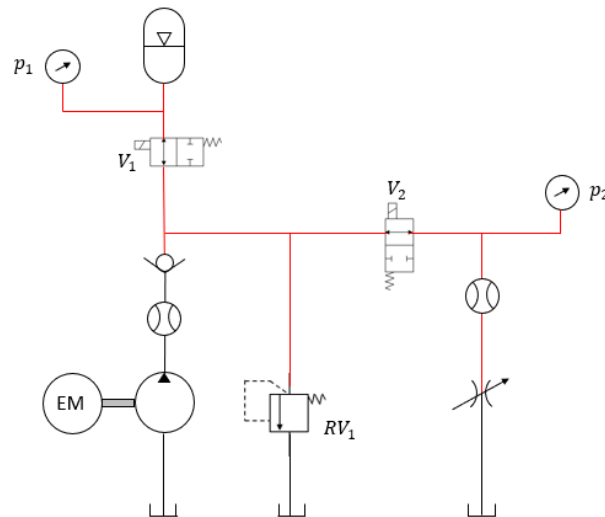


Figure 4.5. Hydraulic test bench during discharging mode.

To discharge the accumulator, the valves V1 and V2 are open, while the proportional valve of the orifice is partially open. The measured variables during discharge mode are the pressure and the flow rate just before the orifice, with these variables it is possible to calculate the instantaneous power available to be used from the accumulator. The output energy can be calculated, and the efficiency of the hydraulic accumulator can be derived. As a reference, the results for a single test is shown in figure 4.6.

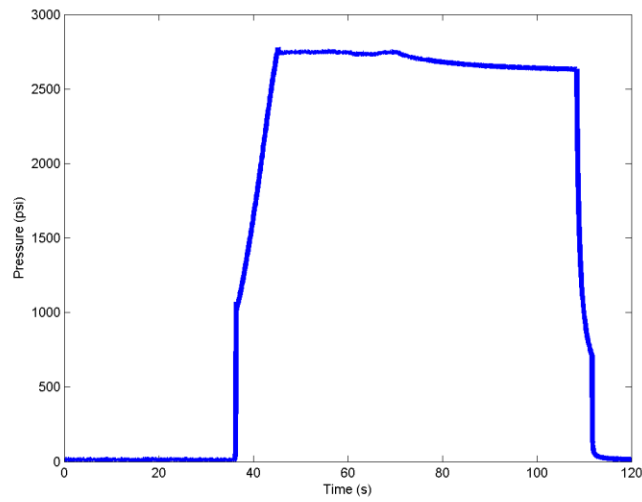


Figure 4.6. Pressure in the accumulator during the charging and discharging process.

The results for pressure and flow rate while charging are shown in figure 4.7.

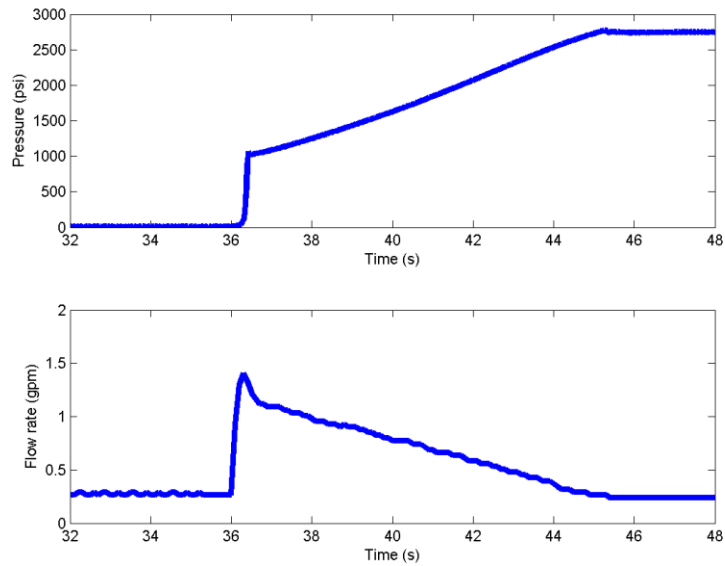


Figure 4.7. Pressure (top) and flow rate (bottom) while charging.

The results for pressure (top) and flow rate (bottom) while charging are shown in figure 4.8.

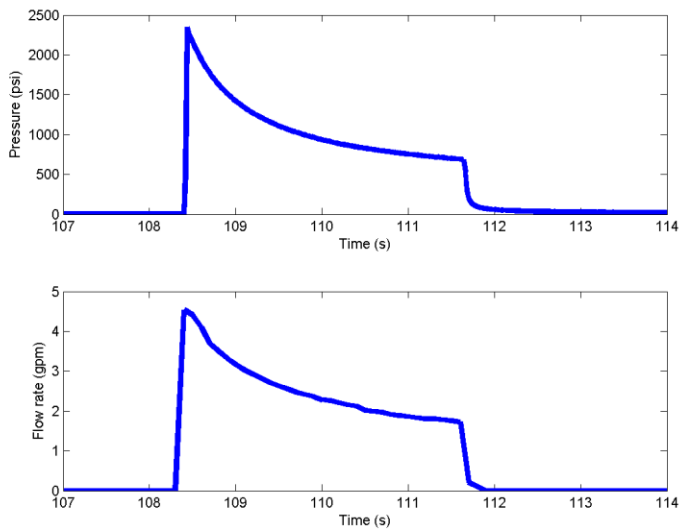


Figure 4.8. Pressure and flow rate while discharging.

Several charge and discharge cycles were performed to calculate the efficiency of the hydraulic accumulator. A detailed explanation of the results is included in the next sections.

4.2 Energy tests for an arrangement of ultracapacitors

A test bench for an arrangement of ultracapacitor was made to calculate the performance of this energy storage device. A schematic representation of the test bench presented in figure 4.9.

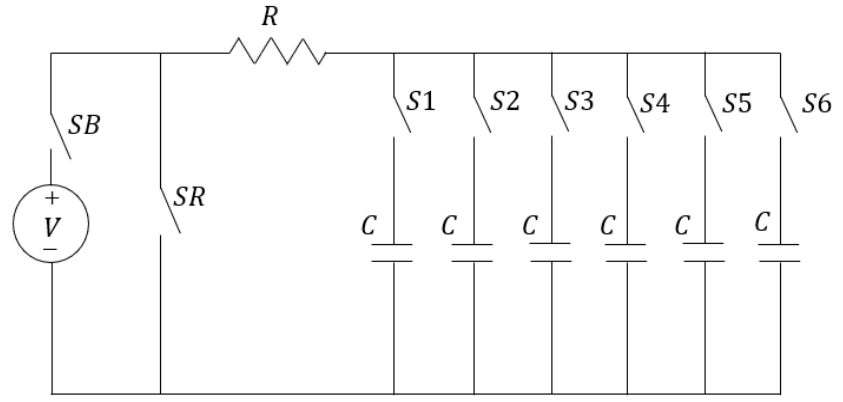


Figure 4.9. Schematic representation of the test bench for ultracapacitors.

This test bench was designed to measure the flow of energy through the ultracapacitors while charging and discharging. The resistance is made with rheostats connected, this makes the value of the resistance variable and easy to adjust. The ultracapacitor arrangement has six cells connected in series in a balancing board and six boards connected in parallel, so the total number of ultracapacitors used is 36. This number was selected based on the calculations for energy storage capacity for hydraulic accumulators and ultracapacitors. The selection of 36 ultracapacitors makes the energy storage capacity comparable between the two devices.

The number of ultracapacitors used in the electric testbench was chosen to match the energy capacity of the hydraulic accumulator. The energy in the hydraulic accumulator was calculated using equation 4.1:

$$E_{acc} = - \int_{V_o}^{V_f} p dV \quad (\text{Eq. 4.1})$$

Using the ideal gas law, equation 4.1 can be expressed as:

$$E_{acc} = \frac{p_o V_o}{n - 1} \left[\left(\frac{p_o}{p_{max}} \right)^{\frac{1-n}{n}} - 1 \right] \quad (\text{Eq. 4.2})$$

In equation 4.2, p_o is the precharge pressure in the hydraulic accumulator, V_o is the initial gas volume, p_{max} is the maximum pressure, and n is the ideal gas constant. The values used for the calculation of energy capacity in the hydraulic accumulator are shown in table 3.

Table 3. Estimated energy capacity of the hydraulic accumulator.

p_o (psi)	1000
p_{max} (psi)	3000
n	1.4
V_o (liter)	1
E_{acc} (Wh)	1.77

The energy storage capacity of the ultracapacitor arrangement should be equal to the energy estimated with equation 4.2. The energy in an ultracapacitor can be calculated with equation 4.3.

$$E_{ult} = \frac{1}{2} C V_{ut}^2 \quad (\text{Eq. 4.4})$$

In Eq. 4.4, C is the capacitance and V_{ut} is the voltage of the ultracapacitors. The capacitance and the voltage of the arrangement can be calculated as function of the number of cells in series and the number of boards in parallel with equations 4.5 and 4.6.

$$C = \frac{N_B}{N_C} C_{cell} \quad (\text{Eq. 4.5})$$

$$V_{ut} = N_C V_{cell} \quad (\text{Eq. 4.6})$$

The total energy in the ultracapacitor arrangement can be calculated with equation 4.7.

$$E_{ult} = \frac{1}{2} C_{cell} V_{cell}^2 (N_B N_C) \quad (\text{Eq. 4.7})$$

With six cells connected in series in a single board, and six boards connected in parallel it is possible to have a similar energy capacity in both systems. The energy storage capacity for the ultracapacitors is shown in table 4.

Table 4. Estimated energy capacity for the ultracapacitors

$C_{cell} (F)$	50
$V_{cell} (V)$	2.7
N_B	6
N_C	6
$E_{ult} (Wh)$	1.82

The current and the voltage in the ultracapacitors were measured during the charging and discharging cycles. Several experiments like the one described in this section were made to calculate the efficiency and performance of the ultracapacitor arrangement. A detailed explanation of the results is included in the next sections.

4.3 Results for the hydraulic accumulator

Power in the accumulator can be calculated as the product of the pressure and the flow rate. These variables were measured during charging and discharging. The results for the energy calculation and the energy efficiency for the hydraulic accumulator are shown in table 5.

Table 5. Results for energy calculation in the hydraulic accumulator.

Energy saved while charging	$1.308 \pm 0.003 \text{ Wh}$
Energy released while discharging	$1.147 \pm 0.005 \text{ Wh}$
Energy efficiency	$87.7 \pm 0.6 \%$

4.4 Results for the ultracapacitors

The tests in the ultracapacitor test bench were made changing the amount of boards connected and the resistance used in the circuit. For each of the possible six board configurations, five different values of resistance were used. So, starting with just one board of six ultracapacitors, the charge and discharge tests were performed five times, in each time the resistance was different. In total, thirty experiments were conducted for charging and thirty experiments were conducted for discharging. With the results of these tests, it is possible to calculate the energy in the ultracapacitors and the efficiency. The results for energy calculations in the ultracapacitors are presented in table 6.

Table 6. Results for energy calculation in the hydraulic accumulator.

	Number of boards connected in parallel											
	1		2		3		4		5		6	
	Value	Error	Value	Error	Value	Error	Value	Error	Value	Error	Value	Error
Energy saved while charging (Wh)	0.31	0.01	0.63	0.02	0.92	0.03	1.24	0.04	1.61	0.05	1.89	0.06
Energy saved while discharging (Wh)	0.25	0.01	0.50	0.01	0.76	0.02	0.97	0.03	1.29	0.04	1.47	0.05
Energy efficiency	77.46	2.33	77.2	2.7	80.75	3.3	78.99	3.91	80.4	4.73	77.74	5.42

4.5 Comparative results

The results for energy density and power density are presented in table 7.

Table 7. Variable comparison for different energy storage systems

	Energy/vol (Wh/m ³)	Energy/mass (Wh/kg)	Cost/Energy (US\$/Wh)	Power/Vol (kW/m ³)	Power/mass (kW/kg)	Cost/Power (US\$/kW)
Battery	195144.0	115.2	0.45	325.24	0.192	271
Ultracapacitor	2539.7	2.72	138.67	2588	2.21	217
Accumulator	1227	0.2884	404.68	7548	2.69	75

The radar plot presented in figure 4.11 is used to better visualize these results. The radar plot shows the results in a scale from 0 to 10 for the three energy storage systems used in this study.

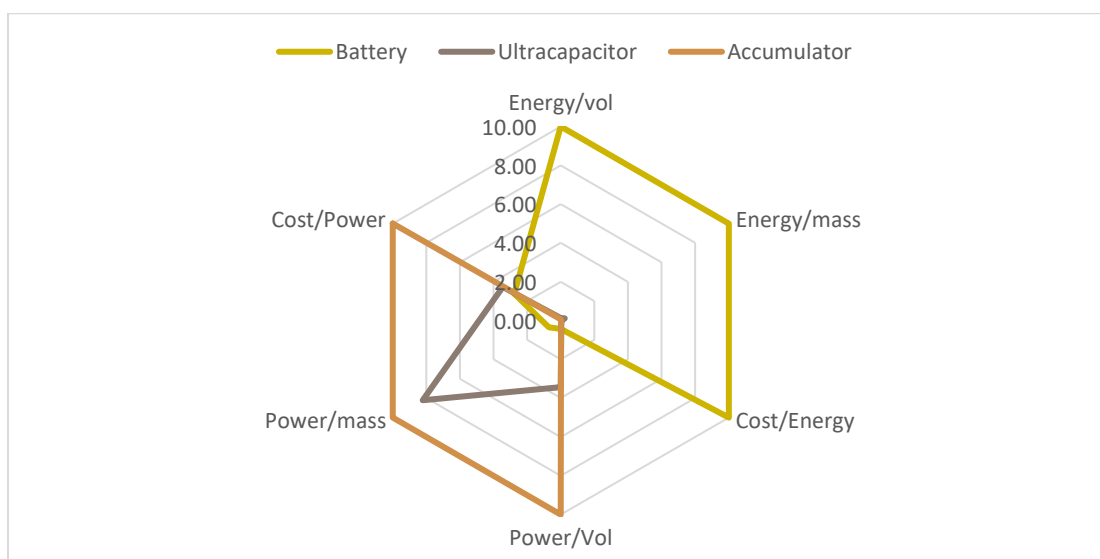


Figure 4.10. Radar plot comparing three energy storage systems.

From the radar plot it is possible to see that the energy side of the plot is almost covered by the battery. None of the other two systems can compete against the battery in terms of energy storage. On the other hand, the hydraulic accumulator covers the power part of the plot. That means that the hydraulic accumulator is the best system to provide power. A comparison between the hydraulic accumulator and the ultracapacitor is shown in figure 4.12.

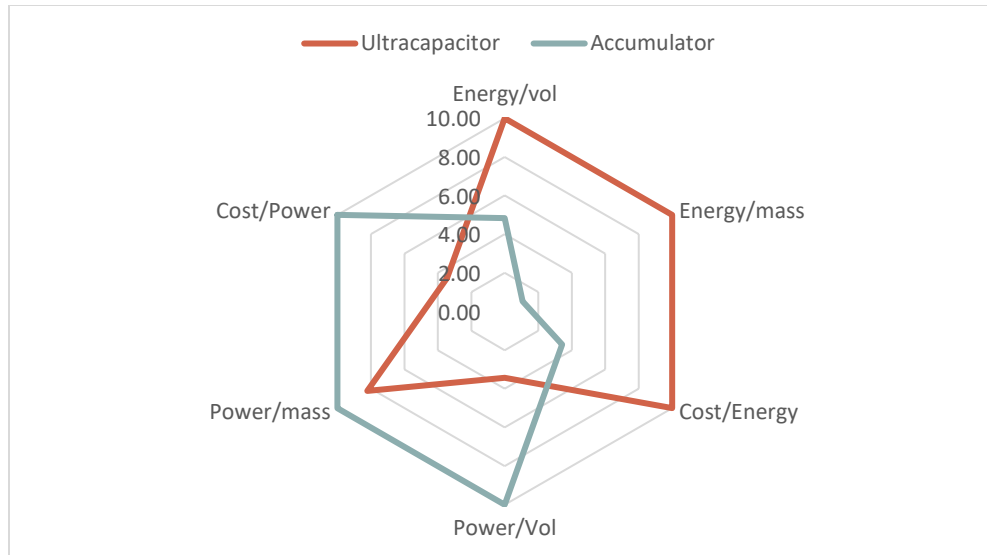


Figure 4.11. Radar plot comparing ultracapacitors and hydraulic accumulators.

From figure 4.12 it is possible to see that the hydraulic accumulator is better than the ultracapacitor in the power side of the plot, while the ultracapacitor is better in the energy side of the plot, but the battery is better than these two systems for storing energy. It is important to mention that the energy efficiency for the ultracapacitor was around 79% and the energy efficiency of the hydraulic accumulator is 87.7%. This improvement in energy efficiency and the better power density compared with ultracapacitors, can be a determining factor to choose a hydraulic system over an electric system for a specific application when needing to rapidly charge or discharge the energy storage devices, such is the case for regenerative braking.

CHAPTER 5. NUMERICAL MODEL OF THE TESTBENCH

A numerical model of the testbench was implemented in order to understand the physical behavior of the system. The numerical model has three different sub models: the prime mover model, the hydraulic system model, and the load simulator model. Also, a control algorithm model was implemented.

5.1 Prime mover model

The prime mover of the system is an AC electric motor which main source of power is a DC battery. There is an inverter between the battery and the electric motor, and there is also a PWM controller to adjust the angular speed in the motor. The electric motor is a brushless dc motor, which is a common name for a permanent magnet ac machine. This name is given because the driving inverted is controlled in such a way that the terminal characteristics of the electric machine are similar to the characteristics of a dc motor. The model of the prime mover has two parts: the model of the inverter and the model of the electric motor. The permanent magnet ac motor driving circuit is shown in figure 5.1.

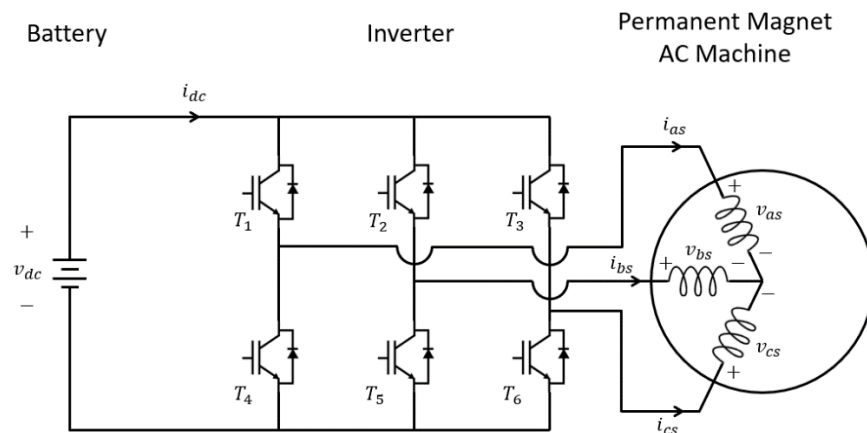


Figure 5.1. Driving circuit for the permanent magnet ac motor

The circuit shown in the figure has a six-stepped inverter, which is one of the possible strategies to generate the signals required to control the inverter. The on/off condition of the logical gates

T_1 to T_6 depends on the rotor position. The switching signals for the logical gates are shown in figure 5.2.

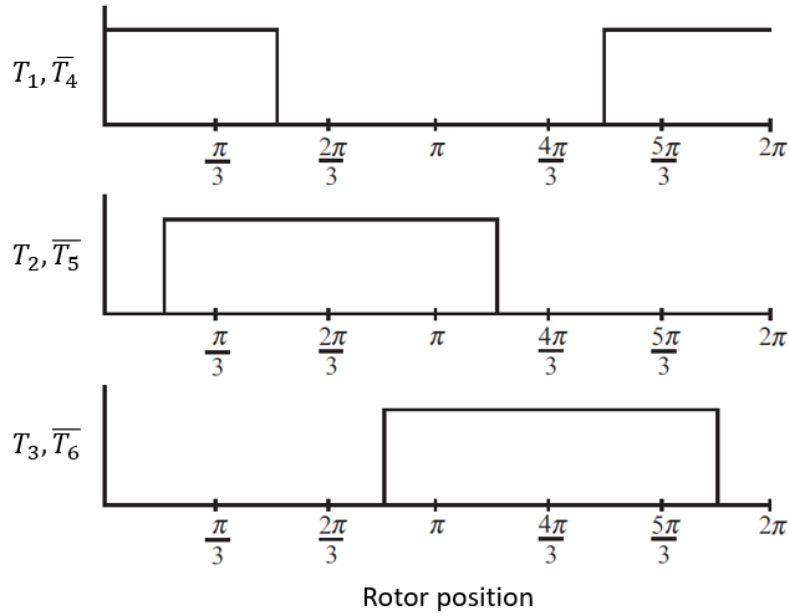


Figure 5.2. Switching signals for the logical gates

In the electric motor, the values of v_{as} , v_{bs} , and v_{cs} depend on the state of the logical gates. The variables in the electric motor can be written in rotor reference-frame variables using equation 5.1. In which f is a general function that could be the voltage, the current or the flux linkages.

$$\begin{bmatrix} f_{qs} \\ f_{ds} \\ f_{os} \end{bmatrix} = \frac{2}{3} \begin{bmatrix} \cos \theta & \cos(\theta - 120^\circ) & \cos(\theta + 120^\circ) \\ \sin \theta & \sin(\theta - 120^\circ) & \sin(\theta + 120^\circ) \\ 1/2 & 1/2 & 1/2 \end{bmatrix} \begin{bmatrix} f_{as} \\ f_{bs} \\ f_{cs} \end{bmatrix} \quad (\text{Eq. 5.1})$$

The current in the rotor-reference frame can be calculated with equation 5.2.

$$I_{ds}^r = \frac{\omega_r L_q}{r_s} I_{qs}^r \quad (\text{Eq. 5.2})$$

The voltage is calculated with equation 5.3.

$$V_{qs}^r = \left(\frac{r_s^2 + \omega_r^2 L_q L_d}{r_s} \right) I_{qs}^r + \omega_r \lambda_m^r \quad (\text{Eq. 5.3})$$

Then, the electric torque in the motor is given by equation 5.4

$$T_e = \left(\frac{3}{2} \right) \left(\frac{P}{2} \right) \left(\frac{r_s \lambda_m^r}{r_s^2 + \omega_r^2 L_q L_d} \right) (V_{qs}^r - \omega_r \lambda_m^r) \quad (\text{Eq. 5.4})$$

Now, applying the fundamental principle of dynamics in a rotor, we can have an equation to couple the electric torque and the torque in the hydraulic pump. The mechanical behavior of the electric motor shaft is modelled with equation 5.5.

$$J \frac{d\omega}{dt} = T_e - T_{HP} - f\omega \quad (\text{Eq. 5.5})$$

The model for the prime mover described in this section was implemented in Simulink. The Simulink model for the inverter is shown in figure 5.3.

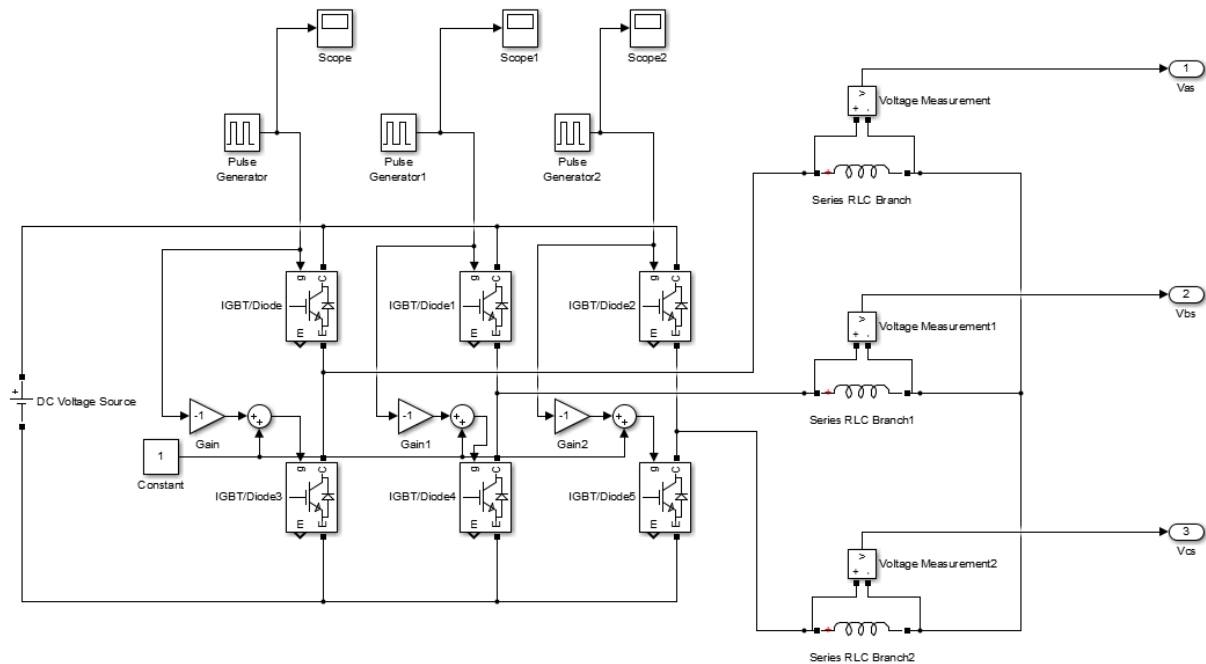


Figure 5.3. Simulink model of the inverter.

The outputs of the inverter model are the voltages v_{as} , v_{bs} , and v_{cs} , which are the inputs for the model of the electric motor. The torque in the hydraulic pump is also an input for the model of the electric motor. The outputs of the electric motor model are the electric torque and the shaft speed. The model of the electric motor is shown in figure 5.4.

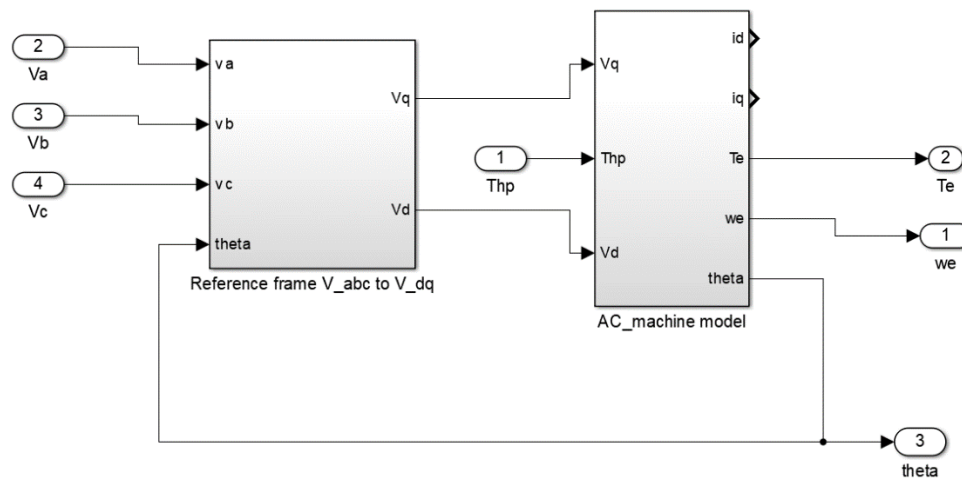


Figure 5.4. Simulink model of the electric motor

The subsystem “Reference frame V_abc to V_dq” is used to apply the reference frame conversion to facilitate the calculations for the electric motor, so this subsystem is using equation 5.1. On the hand, the subsystem “AC_machine model” is solving equation 5.2, 5.3, 5.4 and 5.5 to calculate the electric torque and the angular speed. The subsystem is shown in detail in figure 5.5.

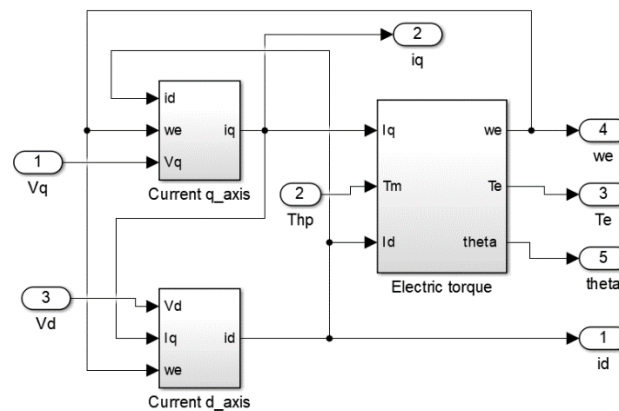


Figure 5.5. Subsystem “AC_Machine model”

The electric torque and the shaft speed, which are the outputs of the electric motor model, are the inputs for the model of the hydraulic pump, which is described in the next section.

5.2 Hydraulic system modeling

The hydraulic system model has three main parts: the model of the hydraulic pump, the model of the hydraulic motor, and the model of the hydraulic accumulator. The hydraulic pump is propelled by the electric motor, these two devices are connected by a mechanical device which in the case of the testbench studied in this thesis is a chain. The flow coming from the pump goes to the hydraulic motor, which converts the hydraulic power into mechanical power in its shaft. This mechanical power is the input of the electric generator that is used as a load.

A hydraulic pump is a device used to convert mechanical power from a prime mover into hydraulic power that can be used to perform work. The energy conversion process is not perfect, there are inefficiencies associated with the friction between the mechanical components of the system, and fluid leakage because of the gaps of the internal parts of the pump. It is important to consider the energy losses in the hydraulic pump in order to correctly estimate the performance of any hydraulic system. The efficiency of a hydraulic pump depends on many factors including shaft speed, fluid pressure, viscosity of the fluid, temperature of the fluid, and geometry parameters of the pump. Moreover, the fluid dynamics inside the hydraulic pump is a complex dynamic process that is difficult to model. A numerical model that considers all the possible sources of inefficiencies in a hydraulic pump could have a huge computational cost that slows down the design and analysis process of a hydraulic system.

Among all the numerical models of efficiency in hydraulic pumps there are three main categories: empirical models, analytical models, and physical models. In the work of Kohmascher (Kohmascher, 2008; Kohmascher et al., 2007) a comparison of the historical models for efficiency was made and it is possible to find a definition for each kind of model. Among the historical models it is possible to find the work of Wilson (Wilson, 1946) in which the concepts of mechanical and volumetric efficiencies were introduced. Regarding the general definitions of each type of model, empirical models are just curve fits that require huge amounts of data. Analytical models use

coefficients to fit limited data, but also including numerical models of the physical behavior of the hydraulic pump. The physical models are based on relating the performance of the hydraulic pumps with their physical dimensions such as gap areas.

Regarding empirical models, one of the most recent examples can be found on the work of Mikeska and Ivantysynova (Mikeska & Ivantysynova, 2002) in which an empirical model called “Polymod” was created. In this study, the mechanical and volumetric losses are modeled, not the efficiencies. The model uses three parameters to fit large amount of data: displacement, pressure, and speed. Another example of empirical model can be found in the work of Dorey (Dorey, 1988), in this study non-linear terms are included in the models and the effects of including these terms are explained.

For analytical models, in which limited data is used, one example is the work of McCandlish and Dorey (McCandlish & Dorey, 1984) in which variable loss coefficient were introduced. One of the main benefits of this model was that it only requires nine data points. Zorotti and Nervegna (Zarotti, 1981) derived numerical models for the losses in swash plate units, some of these models contain as many as seven coefficients. Some other studies like Kauranne (Kauranne et al., 2003) emphasizes on the effect of different hydraulic fluids, fluid temperature, fluid viscosity, and fluid properties in general.

In physical models, the numerical modeling of the hydraulic pump is made by using the physical properties of the device such as gap areas, dimensions of the pump, and dynamic models of the moving parts. In the work of Johnson and Manring (Johnson & Manring, 1994) a model of the torque was presented for a variable displacement axial piston pump, this model does not address directly performance or efficiency but it explains the behavior of the internal parts of the pump. Some other studies have derived full body diagrams and dynamic models for the vanes in pumps and motors in different portions of rotation (Hibi & Ichikawa, 1976; Inaguma & Hibi, 2005), the method used could be extended to piston pumps. Some other examples of physical models are the studies developed by Schlosser (Schlosser, 1961, 1968) in which no coefficients are used to fit experimental data, one drawback of this study is that there is no space for improvement.

The dynamic characteristics of the electric motor, the hydraulic pump and the hydraulic motor are modeled with equations 5.6, 5.7, and 5.8.

$$\text{Electric motor} \quad J_{EM}\dot{\omega}_{EM} = T_e - T_{hp} \quad (\text{Eq. 5.6})$$

$$\text{Hydraulic pump} \quad J_{hp}\dot{\omega}_{hp} = T_{hp} - M_{hp} \quad (\text{Eq. 5.7})$$

$$\text{Hydraulic motor} \quad J_{hm}\dot{\omega}_{hm} = M_{hm} - T_{hm} \quad (\text{Eq. 5.8})$$

In these equations, J is the mass inertia of the component, T is the mechanical torque in the component, and M is the hydraulic torque. The hydraulic torque in the pump and the hydraulic motor are modeled with equations 5.9 and 5.10.

$$M_{hp} = \Delta P D_{hp} / \eta_{m,p} \quad (\text{Eq. 5.9})$$

$$M_{hm} = \Delta P D_{hm} \eta_{m,m} \quad (\text{Eq. 5.10})$$

In equations 5.9 and 5.10, the variable ΔP is the pressure drop in the system, D is the displacement and η_m is the mechanical efficiency. The flow rate in the pump and the hydraulic motor is calculated with equations 5.11 and 5.12.

$$Q_{hp} = \omega_{hp} D_{hp} \eta_{v,p} \quad (\text{Eq. 5.11})$$

$$Q_{hm} = \omega_{hm} D_{hm} / \eta_{v,m} \quad (\text{Eq. 5.12})$$

The efficiency terms in equations 5.9 to 5.12 are a function of the pressure and the flow rate. To create these functions for the efficiency, the information available in the datasheets of the hydraulic devices were used. Regarding the hydraulic accumulator, an adiabatic process was assumed for the model. Also, it is assumed that nitrogen gas in the accumulator follows ideal-gas laws. Taken these assumptions into account, we can write equations 5.13 and 5.14 to model the accumulator.

$$E_{acc} = \frac{p_0 v_0^n}{1-n} [v_2^{n-1} - v_1^{n-1}] \quad (\text{Eq. 5.13})$$

$$p_1 v_1^n = p_2 v_2^n \quad (\text{Eq. 5.14})$$

The Simulink model of the hydraulic system is shown in figure 5.6.

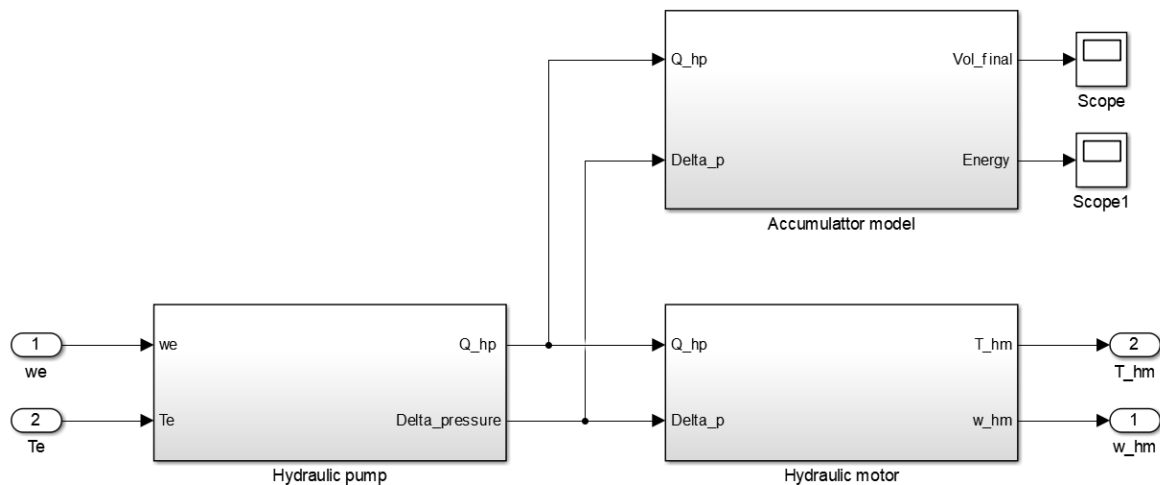


Figure 5.6. Hydraulic system model

The torque and the shaft speed in the hydraulic motor are the inputs for the model of the electric generator.

5.3 Load simulator model

The electric generator is a dc electric machine that can be represented by the schematic shown in figure 5.7.

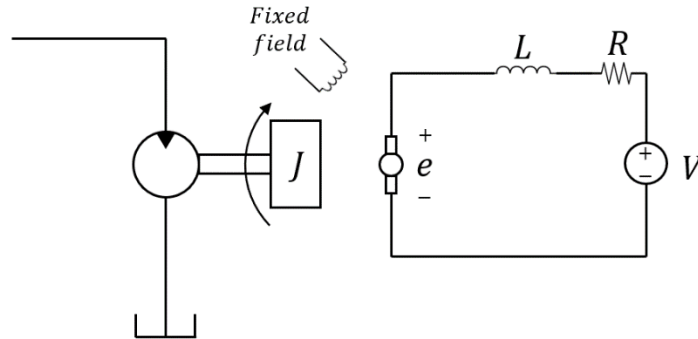


Figure 5.7. Schematic representation of the load simulator

The hydraulic system and the electric system are coupled through the shaft of the hydraulic motor. The system can be modeled from the mechanical point of view and from the electrical point of view, and these two are coupled. Equation (5.15) and (5.16) show the mechanical and electric model, respectively.

$$J\ddot{\theta} + b\dot{\theta} = T_{hm} - T_e \quad (\text{Eq. 5.15})$$

$$L \frac{di}{dt} + Ri = K_v \dot{\theta} \quad (\text{Eq. 5.16})$$

In equation (5.15), T_{hm} is the hydraulic torque from the hydraulic motor, T_e is the electric torque in the electric generator. In equation (5.16), K_v is the voltage constant of the electric generator, R is the armature resistance, and L is the armature inductance. The electric torque and the hydraulic torque can be calculated with equations (5.17) and (5.18)

$$T_e = K_T i \quad (\text{Eq. 5.17})$$

$$T_h = \frac{\Delta p D_p}{2\pi} \eta_m \quad (\text{Eq. 5.18})$$

The current of the electric generator can be expressed as a function of the control signal that is used to adjust to load of the system. A PWM signal is used to adjust the current and the load in the testbench, the relation between the current and the control signal is assumed as linear and is given by equation (5.19).

$$i = K_c u \quad (\text{Eq. 5.19})$$

Equations (5.17), (5.18), and (5.19) were plug into equations (5.15) and (5.16) to obtain equation 5.20 and 5.21.

$$\text{Mechanical equation} \quad J\dot{\omega}_g + b\omega_g = \Delta p D_p \eta_m - K_T K_c u \quad (\text{Eq. 5.20})$$

$$\text{Electric equation} \quad LK_c \frac{du}{dt} + RK_c u = K_v \omega_g \quad (\text{Eq. 5.21})$$

Then, with equations 5.20 to 5.21 it is possible to define a mathematical relation between the control signal u and the pressure in the system. Also, using equation 5.19 it is possible to calculate the current in the electric generator, which is useful to have a relation between the pressure and the current.

After applying the Laplace transform to the above equations, it is possible to have a transfer function between pressure in the hydraulic motor and the control signal of the PWM controller used in the load system. The transfer function is shown in equation 5.22:

$$\frac{\Delta p(s)}{U(s)} = \frac{LK_c J}{K_v D_p \eta_m} s^2 + \frac{RK_c J}{K_v D_p \eta_m} s + \frac{LK_c b + RK_c b + K_T K_c K_v}{K_v D_p \eta_m} \quad (\text{Eq. 5.22})$$

In equation 5.22, it is possible to see different parameters such as dynamics characteristics like the mass inertia (J) and the viscous coefficient of the shaft (b), also some electric parameters such as armature resistance, and armature inductance. There also some constants related with the electric characteristics of the electric generator such as the torque constant that relates the torque and the current, the voltage constant that relates the voltage and the speed, and the control constant,

that relates the current and the control signal. Experimental data was used to determine the value of the parameters used in equation 5.22. The control model implemented in Simulink is shown in figure 5.8.

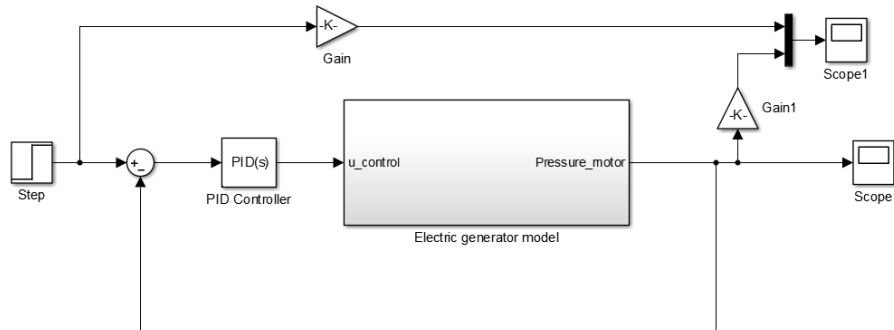


Figure 5.8. Control algorithm model for the electric generator.

CHAPTER 6. TESTBENCH IMPLEMENTATION

6.1 General description

The testbench was designed to simulate different conditions of operation for electro-hydraulic applications. The testbench can operate as a hydrostatic transmission, which can be used to transfer power from a prime mover to an actuator connected to a load. This testbench can work as a system to charge the hydraulic accumulator and store energy as pressure and release this energy to move the actuator. This feature is useful to measure the performance of the system when it is working under different operating conditions.

The testbench has different subsystems that are working and controlled simultaneously. The first subsystem is the prime mover, which is composed of a permanent magnet DC motor which is powered with a DC battery. These two devices are connected with an inverter, which allows controlling the angular speed of the electric motor. The second subsystem is the hydraulic system, which is basically a fixed displacement hydrostatic transmission which is used to transmit power from the prime mover to the actuator, which in this case is a hydraulic motor. The third subsystem is a load simulator, which is used to dissipate the energy of the system and simulate different load conditions. This load simulator is made with an electric generator connected to a set of rheostats. The amount of power dissipated with the electric generator is controlled by adjusting the current output with a PWM controller. The subsystems are presented in the figure 6.1.

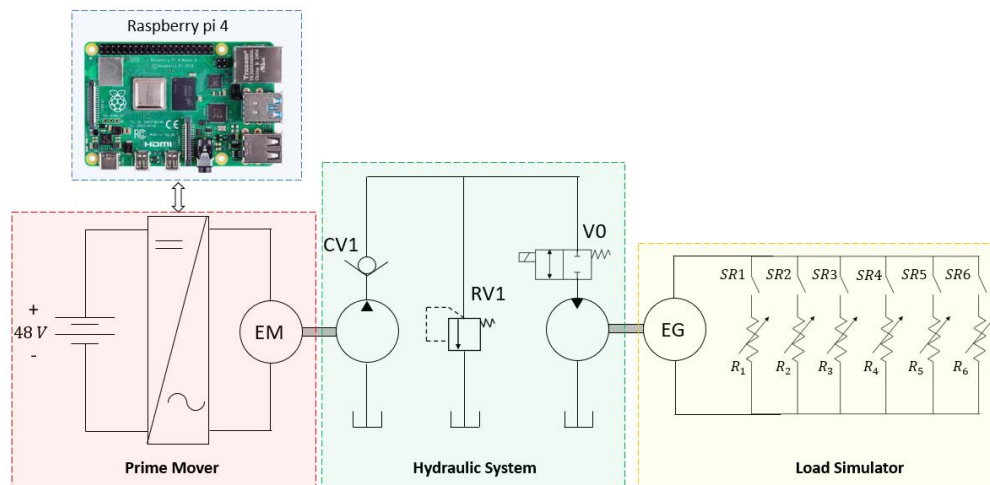


Figure 6.1. Subsystems in the testbench

All the performance variables in the subsystems of the testbench are measured using a centralized software that takes all the data from the sensors and makes adjustments according to the output signals. The instrumentation system is programmed in a Raspberry Pi 4.

6.2 Prime mover

The prime mover subsystem is presented in figure 6.2. The main source of energy of the prime mover is a 48 VDC battery pack, specially designed for mobile applications. The characteristics of the battery are presented in table 8.

Table 8. Battery parameters

Nominal voltage	48 V
Battery composition	LiFePO4
Battery Capacity	17 Ah
Charging cut-off voltage	58.4 V
Discharging cut-off voltage	33.6 V
Instantaneous Maximum Discharge Current	≤ 60 A
Rated charging current	4 A
Maximum charge current	10 A

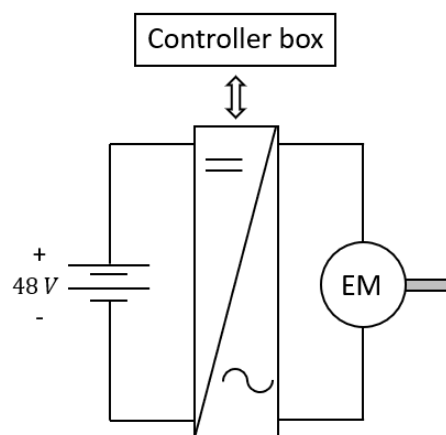


Figure 6.2. Schematic representation of the prime mover of the testbench

The terminals of the battery are connected to the DC/AC inverter, which is connected to a controller box which changes the angular speed in the electric motor. The inverter is connected to a circuit that is designed to adjust the signal of the electric motor with the Raspberry Pi 4. The battery, the inverter and the circuit design are presented in figures 6.3, 6.4 and 6.5 respectively.



Figure 6.3. LiFePO4 Battery pack used in the testbench



Figure 6.4. Inverter used in the testbench

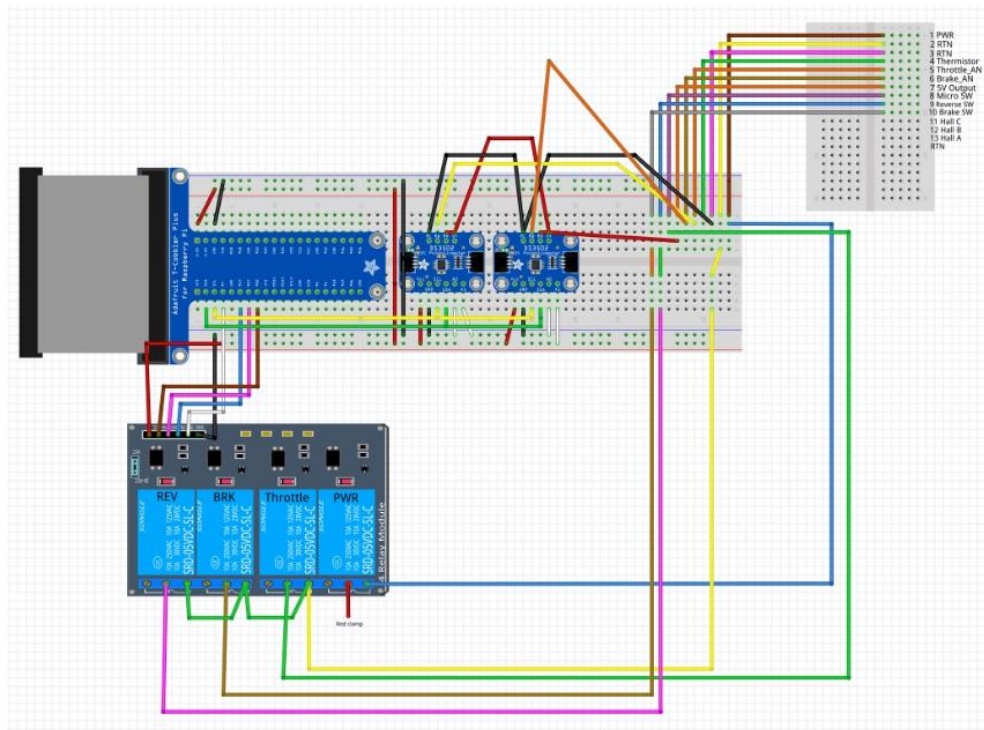


Figure 6.5. Circuit design schematic and connection to Raspberry Pi 4.

The inverter and the circuit are used to control the speed in the electric motor. The shaft of the electric motor is connected to the shaft of the hydraulic pump. The variables measured in the prime mover system are the current from the battery, the voltage from the battery, and the angular speed of the electric motor. The circuit and the devices used to measure these variables are described in depth in chapter 6.5.

6.3 Hydraulic system

The schematic of the hydraulic system is presented in figure 6.6 and the principal characteristics of the hydraulic devices are presented in table 9.

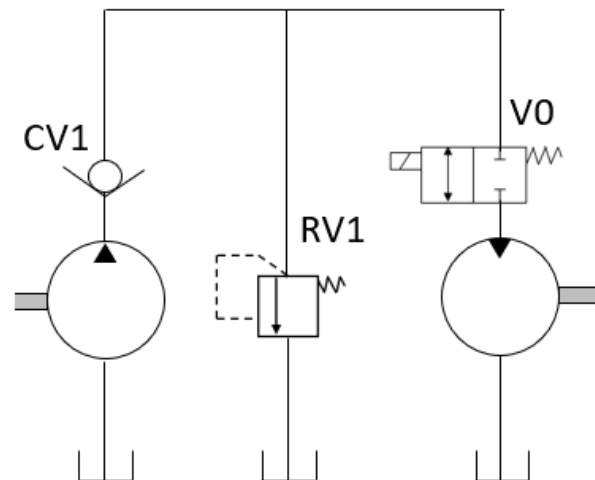


Figure 6.6. Schematic representation of the hydraulic system

Table 9. Main characteristics of the hydraulic system

Device	Reference	Characteristics
Hydraulic pump	GP-F20-12-P-A	Disp: 12 cm^3/rev Max. Flow: 40 L/min Max. Pressure: 252 Bar
Hydraulic motor	MGG20010-BA1A3	Disp: 3.57 cm^3/rev Max. Flow: 18 L/min Max. Pressure: 137 Bar
Flow meter	FlowTech FSC 375	Max. Pressure: 6 kpsi Max. Flow: 26.45 L/min
V1 to V5	Hydraforce 12 V DC NC solenoid valve	Max. Flow: 56.7 L/min Max. Pressure: 3 kpsi
Pressure gage	Wika A-10	Max. Pressure: 5 kpsi Signal output: 4 to 20 mA
Hydraulic accumulator	Parker A2N0058D1K	Capacity: 58 in^3 Max. Pressure: 3 kpsi Precharge pressure: 1 kpsi

The variables that are measured during the operation of the hydraulic system are the angular speed in the hydraulic pump, the flow rate in the system, the pressure in the input of the hydraulic motor, the torque in the hydraulic motor, and the angular speed in the hydraulic motor. With these variables, it is possible to determine the performance of the hydraulic system under any given conditions of operation. The sensors and the instrumentation system used to measure these variables are described in deep in section 6.5.

6.4 Load simulator

The schematic of the load simulator is presented in figure 6.7 and the principal characteristics of the devices used in the load simulator are presented in table 10.

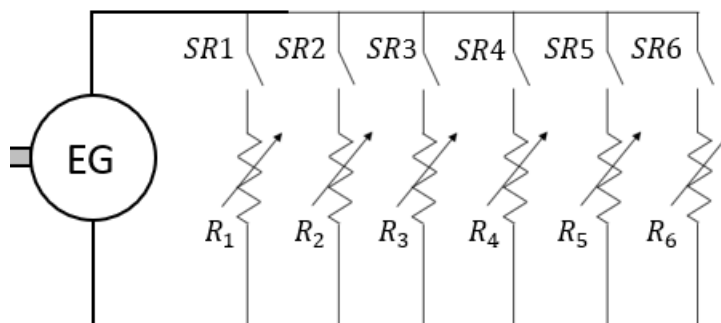


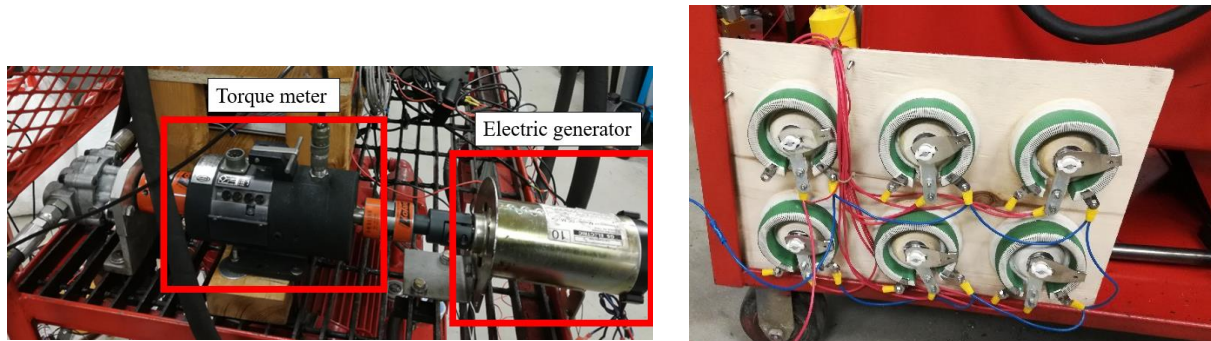
Figure 6.7. Schematic representation of the load simulator

Table 10. Main characteristics of the load simulator

Device	Reference	Characteristics
Electric generator	B4CPM-102T	Rated power: 2.5 hp Max. Current: 18 A Max. Speed: 6700 rpm
Rheostats	Electronics-Salon Power Wirewound Potentiometer, rheostat, variable resistor	Rated power: 200 W Resistance: 50 ohms Shaft diameter: 6 mm
Relay	JBtek 8 Channel DC 5V Relay Module for Arduino Raspberry Pi DSP AVR PIC ARM	5V 8-Channel relay interface board. Driver current: 15-20 mA
Torque meter	Lebow Shaft Torque Sensor Mod. 1114-106	Max. Torque: 100 lb.in Max. Speed: 16000 rpm
PWM Speed controller	RioRand Upgraded 6V-90V 15A DC Motor Pump Speed Controller	Max. Current: 15 A Working voltage: 6V – 90V

The variables measured in the load simulator are the torque in the electric generator, the current, the voltage and the shaft speed. With these variables it is possible to determine the performance of the load simulator. It is possible to estimate the efficiency of the energy conversion process with the variables measured in the load system. The load simulator is shown in figure 6.8. The sensors

and the instrumentation system used to measure these variables, are described in depth in section 6.5.



Torque meter and electric generator

Rheostats used to dissipate the energy in the load simulator.

Figure 6.8. Load simulator of the testbench

6.5 Instrumentation

The instrumentation and control algorithm for the testbench were implemented using python programming language and Raspberry Pi 4. The circuits used for the instrumentation and control system were developed using open source hardware and electronic modules. The instrumentation and control system were designed to adjust the accelerator input as a function of a given driving schedule and then adjust the speed in the prime mover of the system. The pressure control in the system is achieved by adjusting the amount of power dissipated in the load simulator, the power dissipated was controlled by adjusting the signal in a PWM controller. Analog to digital converters were used for the data acquisition system. The pressure transducers, the flow meters, the current sensors, the voltage sensor, and most of the sensors used to measure the performance variables of the system are analog devices, so it is necessary to convert the analog signal into digital signal in order for it to be processed and recorded with Python and the Raspberry Pi 4.

6.5.1 Accelerator Input

The accelerator input in the testbench was a control box that was connected to the DC/AC inverter. This control box had two potentiometers: one for the forward acceleration and one for the reverse acceleration. The control box has four switches to activate the power input to the electric motor,

the throttle input, the braking input, and the reverse operation. The original control box connected to the inverter is shown in figure 6.9.



Figure 6.9. Original control box.

This control box is an analog device that is controlled manually. The output signal of this control box is sent to the inverter with a cable with multiple outputs. A circuit to replace this control box was designed. The main considerations for the new design of the controller box were the need to control the testbench using a main program from the computer, the ability to accurately control the speed in the prime mover, and the ability to follow different driving schedules. In order to achieve these requirements, a Raspberry Pi 4 computer was used to control the accelerator input signal in the testbench. The analog potentiometers used in the original control box were replaced by digital potentiometers that can be controlled with the Raspberry Pi 4. The switches used in the original control box were replaced with digital relays that can be activated using the main program created for control the system. In order to have the same configuration, the new design was constructed in the same format except digitally. The digital control box is presented in figure 6.9. The circuit design schematic was presented in figure 6.5.

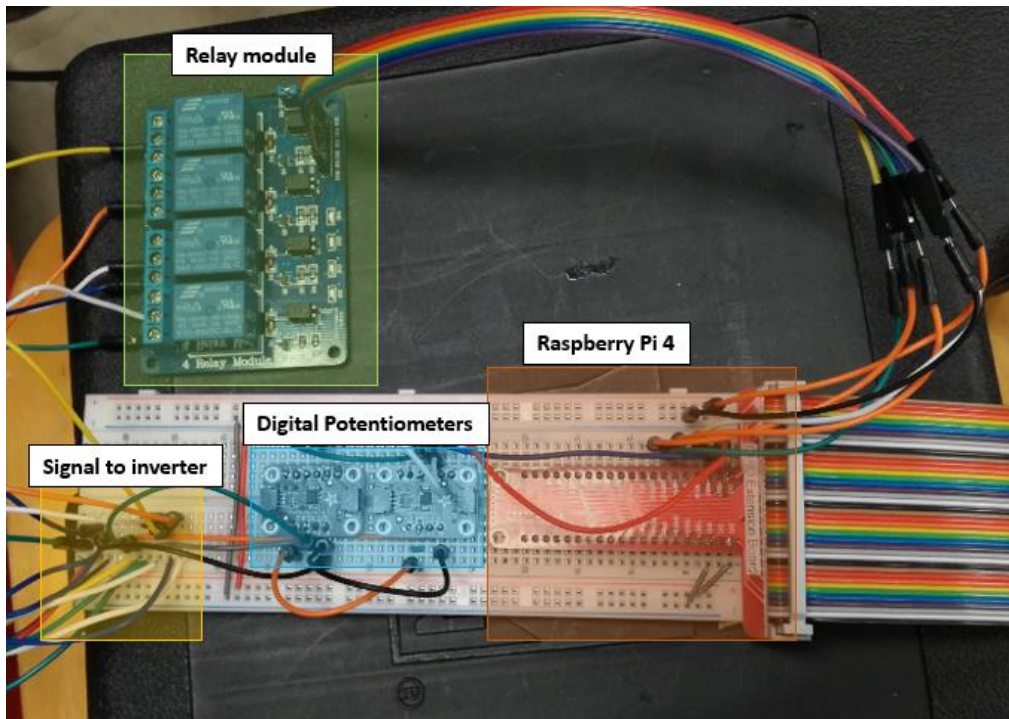


Figure 6.10. Digital control box used in the testbench.

The list of components used in the digital control box are presented in table 11.

Table 11. List of components used in the digital control box.

Device	Reference	Characteristics
Digital potentiometer	Adafruit DS3502 I2C Digital 10K Potentiometer Breakout	Resistance: 0-10 kOhms Voltage input:4.5–15.5 V 7-bit Analog to digital conversion
Relay	JBtek 4 Channel DC 5V Relay Module for Arduino Raspberry Pi DSP AVR PIC ARM	5V 4-Channel relay interface board. Driver current: 15-20 mA
Expansion Board for Raspberry Pi 4	Lebow Shaft Torque Sensor Mod. 1114-106	Max. Torque: 100 lb.in Max. Speed: 16000 rpm
PWM Speed controller	RioRand Upgraded 6V-90V 15A DC Motor Pump Speed Controller	Max. Current: 15 A Working voltage: 6V – 90V

6.5.2 Speed Controller

The hardware designed to control the speed in the system is the digital control box presented and described in section 6.5.1. The Python code used for the speed controller received as an input the desired driving schedule. For the first tests, the driving schedule was a function of the speed in the hydraulic motor. When the speed in the motor is less than the desired speed, then the voltage signal from the potentiometer in the control box is increased, so the speed in the electric motor increases and the flow rate as well, so the speed in the hydraulic motor increases. The digital potentiometers have a resolution of 7-bit, and what that means is that the voltage in these potentiometers don't change continuously, but in predefined step. When the signal of the potentiometer is 1, the voltage is zero and the speed is zero as well. When the signal in the potentiometer is 128, the voltage is 5V and the speed is maximum. The speed controller changes this digital signal to adjust the speed in order to obtain a desired value of the actuator speed.

The flow rate is measured by using a magnetic flow meter that produces a sinusoidal signal with a designated frequency which is related to the flow rate passing by the flow meter. A circuit was designed to convert this sinusoidal signal into a digital signal that can be read by the Raspberry Pi. This circuit has two parts: one part is used to adjust the amplitude of the sinusoidal signal, and the other part is used as a voltage comparator which is zero when the voltage signal is less than 0 V, and is 1 when the signal is greater than 0 V. The schematic representation of the control loop is shown in figure 6.11.

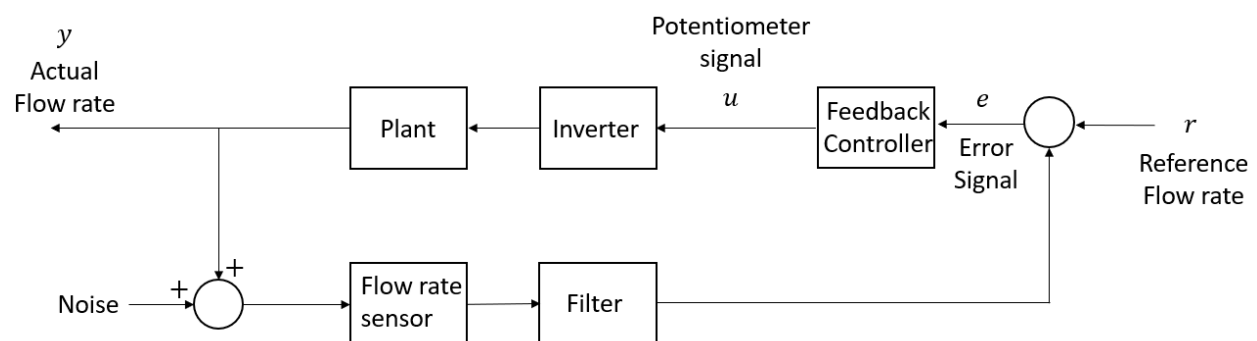


Figure 6.11. Schematic representation of the control loop for the speed in the hydraulic motor.

The actual circuit designed to measure the flow rate is presented in figure 6.12.

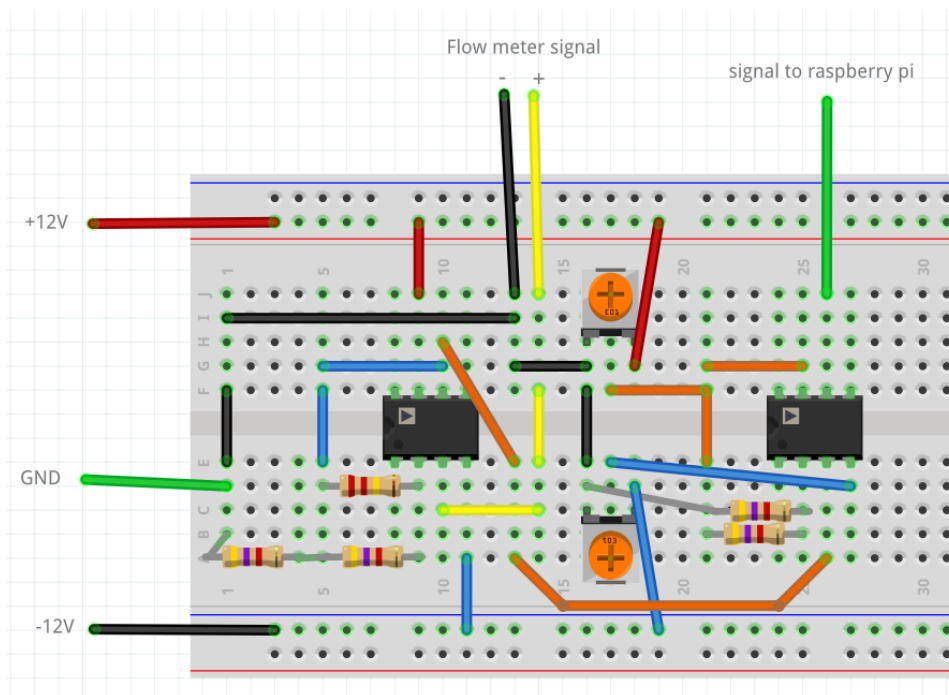


Figure 6.12. Circuit prototype used for the flow rate measurement in the Raspberry Pi 4.

The circuit presented in figure 6.12 can be used to measure the speed in the system. The speed sensors work in a similar way, they produce a sinusoidal signal that needs to be converted into a digital pulse in order to be used in the Raspberry Pi 4. The potentiometers used in the circuit are useful to adjust the amplitude of the signal, so it can be used for many sensors with the same kind of output. It is possible to calculate the frequency of this pulses by using the libraries available on Python. The main devices used for the flow rate signal measurement and their characteristics are listed in table 12.

Table 12. Characteristics used in the flow controller system.

Device	Reference	Characteristics
Flow meter	Flo-Tech FSC 375	Frequency output Max. Pressure: 6000 psi Accuracy: $\pm 1\%$ Calibration: 1600 Hz = 4.25 GPM 200 Hz = 0.53 GPM
Operational amplifier	LM741 Amplifier	Operational Supply voltage: $\pm 22V$ Input voltage: $\pm 15V$

6.5.3 Pressure Controller

The pressure in the testbench is a function of the amount of power that is dissipated in the electric generator. The power dissipated is given by equation 6.1.

$$P_{EG} = V_{EG}I_{EG} \quad (\text{Eq. 6.1})$$

Where P_{EG} is the power in the electric generator, V_{EG} is the voltage, and I_{EG} is the current in the electric generator. The voltage in the electric generator depends on the shaft speed, and the current depends on the load of the system. The shaft speed of the electric generator is the same shaft speed in the hydraulic motor, so the speed in the electric generator is controlled with the speed controller of the prime mover. The current and the pressure in the system are coupled, so the greater the current in the electric generator, the greater the pressure in the hydraulic system. A PWM controller was used to control the current in the electric generator. The signal in the PWM controller is adjusted with a digital potentiometer that is connected to the Raspberry Pi 4. The current produced by the electric generator is dissipated in the rheostats connected in parallel to the generator. These rheostats allow for change in the load of the system, so there are two ways to change the load: either by adjusting the PWM signal or changing the resistance value in the rheostats. The main code in the Raspberry Pi 4 has a function to adjust the PWM signal value in order to change the current in the generator. The schematic representation of the pressure controller hardware is shown in figure 6.13.

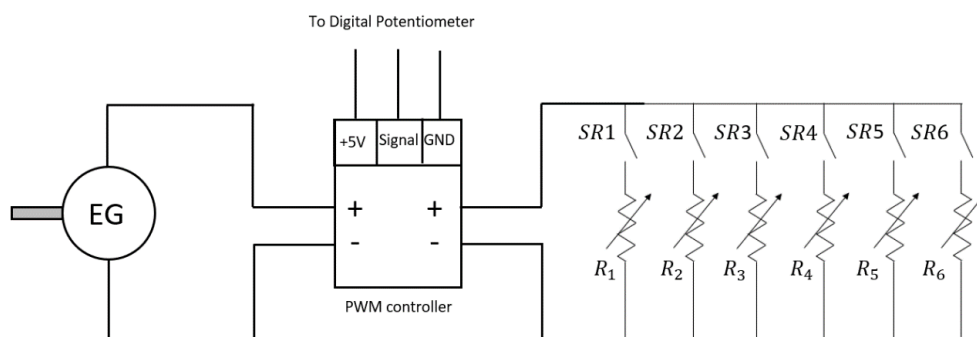
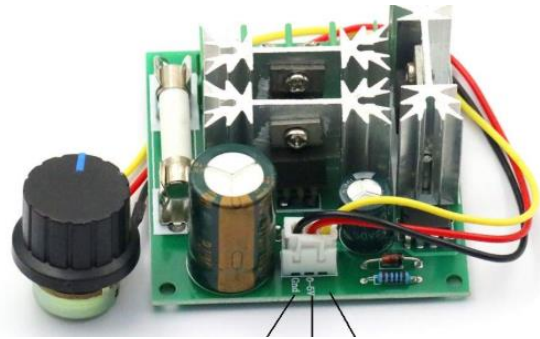


Figure 6.13. Schematic representation of the pressure controller hardware.

The current, the voltage, the shaft speed, and the torque are measured in the system. The pressure controller adjusts the current through the PWM signal and the pressure in the system changes. The main code in the Raspberry Pi 4 received as an input a desired value for pressure and the control algorithm gives as an output from the digital potentiometer signal output that goes to the PWM controller to adjust the current and then the pressure in the system. The generator, the PWM controller, and the rheostats are presented in figure 6.14.



Electric Generator



PWM Controller



Rheostats

Figure 6.14. Devices used in the hardware of the pressure controller

6.5.4 Data Acquisition System

The testbench is equipped with sensors used to measure the performance variables of the system. All the sensors used are analog devices that generate signal values proportional to the actual value of the physical property that is measured. However, the Raspberry Pi 4 computer doesn't have analog ports, so it is necessary to convert the analog signals from the sensors to digital signals that

can be read and used by the Raspberry Pi 4. The device used to make this conversion was the analog to digital converter ADS1015 from Adafruit which is a ready-to-use circuit module for this purpose. It is possible to connect 4 of these devices at the same time for a total of sixteen analog input signals. This device converts the analog signal from -5V to +5V into a 12bit digital signal, which means that the digital converter assigns a value between -4096 to 4096 depending on the analog voltage input. The analog sensors used in the testbench are listed in table 13.

Table 13. Analog sensors used in the testbench

Device	Variable	Reference	Characteristics
Pressure transducer	Pressure in the hydraulic system	Wika Type A-10	Pressure: 0 – 5000 psi Output: 0 – 20 mA Max. Input: 30 V
High current sensor	*Current in the battery *Current in the electric generator	Allegro Microsystems Sensor Current Hall 150A AC/DC	Max. Current: 150 A Sensitivity: 13.3 mV/A Accuracy: $\pm 1.6\%$ Voltage supply: 3V–5.5V
Torque meter	Torque in the hydraulic motor/Electric generator shaft	Lebow Shaft Torque Sensor Mod. 1114-106	Max. Torque: 100 lb.in Max. Speed: 16000 rpm
Voltage divider	*Voltage in the battery *Voltage in the electric genertor	Ceramic resistors	Max. Voltage input: 55 V Max. Voltage output: 5 V Max. Current: 20 mA

The analog to digital converter can work with a frequency of up to 3300 samples per second, which is enough time for the testbench response. The characteristics of the analog to digital converter are presented in table 14.

Table 14. Characteristics of the analog digital converter

Device	Reference	Characteristics
Analog to digital converter	Adafruit ADS 1015	Max. sample freq: 3.3kHz Communication protocol: I2C Resolution: 12bit Analog input voltage: -5V to 5V Max. Input Current: 100 mA

The main code implemented on Python in the Raspberry Pi 4 can take the data and can save the data on a text file that can be postprocessed and analyzed using any software.

6.6 Control algorithm

The control algorithm in the testbench was designed to adjust the actual value of the flow rate and the pressure in the system. This system has multiple inputs and multiple outputs, so the control algorithm was divided in two: one part of the algorithm is controlling the flow rate and the other part is controlling the pressure. One of the benefits of a hydraulic system is that the pressure and the flow in the system are independent, so in theory it is possible to have a constant flow regardless of the pressure in the system. In the real testbench when the flow rate increases, the pressure in the system increases as well. The complete control algorithm diagram is shown in figure 6.15.

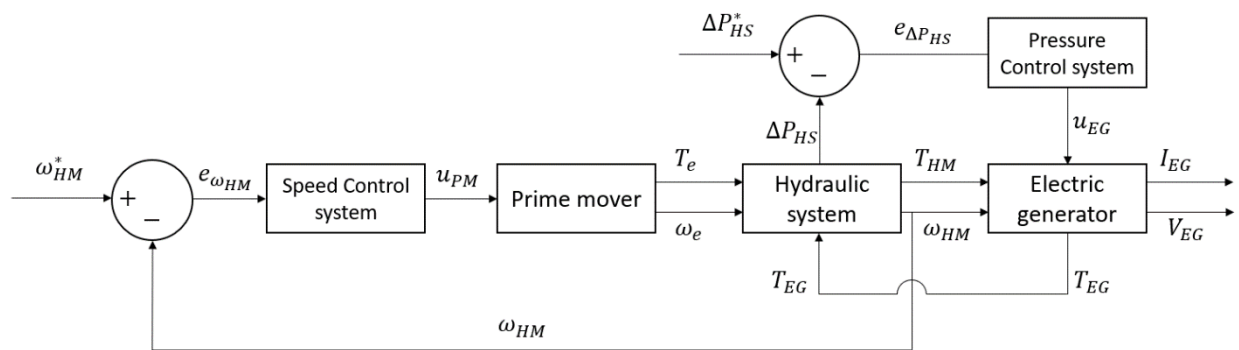


Figure 6.15. Complete control algorithm diagram

The speed controller changes the control signal input in the prime mover to adjust the shaft rotational speed in the electric motor. The pressure controller is used to change the control signal input in the electric generator to adjust the current output and the power dissipated in the system, that will change the pressure in the hydraulic system. Both control algorithms work and are coupled to maintain the desired value of pressure and speed in the hydraulic motor.

6.6.1 Speed Control

The speed control is focused on the electric motor, but the output of this control is the speed of the actuator. This controller receives as an input the difference between the actual (ω_{HM}) and the desired (ω_{HM}^*) shaft speed in the hydraulic motor, and generates as the output the control signal that is going to the prime mover (u_{PM}). The output of the prime mover is the shaft speed (ω_e) and the electric torque (T_e). These two variables and the torque in the electric generator are the inputs for the hydraulic system, and the dynamic behavior of the hydraulic system depends on the way in

which these variables change over time. The actual shaft speed in the hydraulic motor is measured during the operation of the testbench by using a speed sensor embedded in the torque meter used between the hydraulic motor and the electric generator. This speed sensor produces a sinusoidal signal whose frequency is directly proportional to the angular speed. The sinusoidal signal is processed with the circuit described in section 6.5.2. The schematic representation of the control algorithm and the data flow in the speed control are shown in figure 6.16.

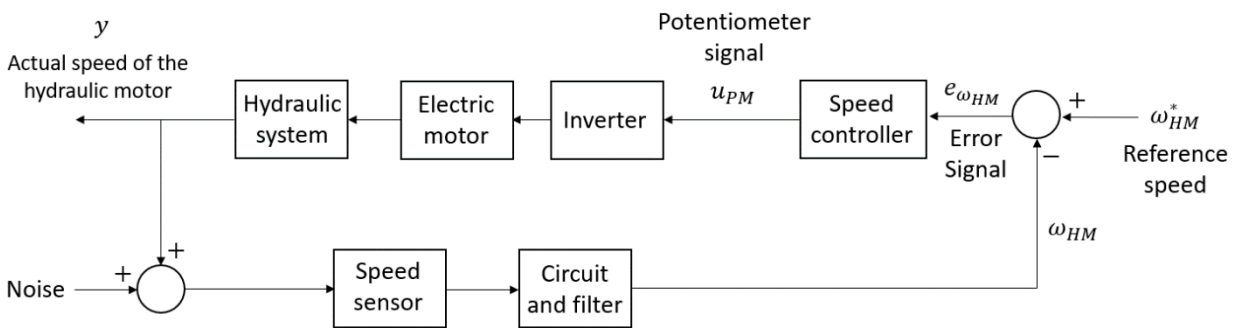


Figure 6.16. Schematic representation of the control algorithm in the speed control

6.6.2 Pressure Control

The pressure control of the testbench is designed to change the PWM signal of the electric generator by using a digital potentiometer. The controller receives as the input the difference between the desired pressure in the system (ΔP_{HS}^*) and the actual pressure (ΔP_{HS}). The controller generates the PWM signal that controls the current in the electric generator (u_{EG}). When the current increases, the load in the system increases and produces an increase in the pressure and a decrease in the shaft speed of the generator. The outputs of the electric generator are electric current, the voltage and the electric torque in the generator. The dynamic behavior of the hydraulic system depends on the way in which these variables change over time. The pressure in the system is measured by using an analog sensor. The signal from the sensor is filtered and then converted into a digital signal by using a circuit designed for that purpose. The schematic representation of the control algorithm and the data flow in the pressure control are shown in figure 6.17.

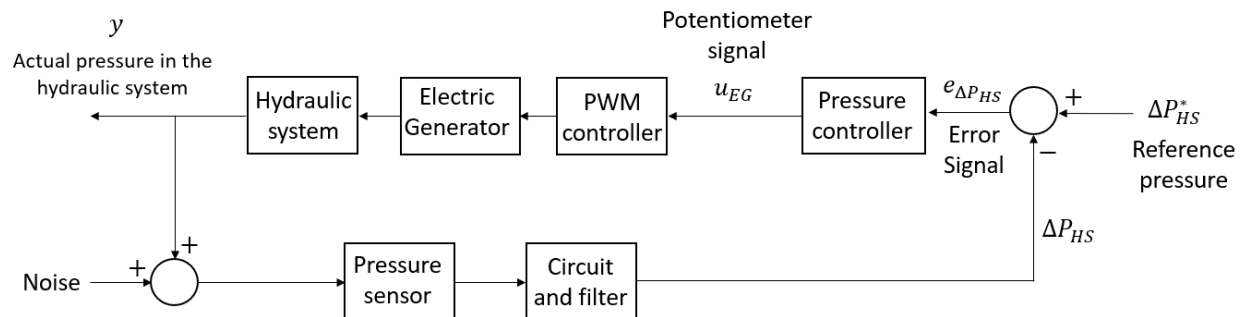


Figure 6.17. Schematic representation of the control algorithm for the pressure control system

CHAPTER 7. RESULTS

The results obtained in this study can be divided into two categories: numerical model results, and the testbench results. The results for these two categories are described in the following sections.

7.1 Numerical Model Results

The Simulink model of the inverter was used to simulate the behavior of the actual inverter used in the testbench. The inverter is used to convert the dc voltage from the battery into the ac voltage that is going to the electric motor. The results for the simulated voltage v_{as} , v_{bs} , and v_{cs} are shown in figure 7.1. The voltage in the reference-frame variables are also shown in figure 7.1. The torque is also shown in this figure.

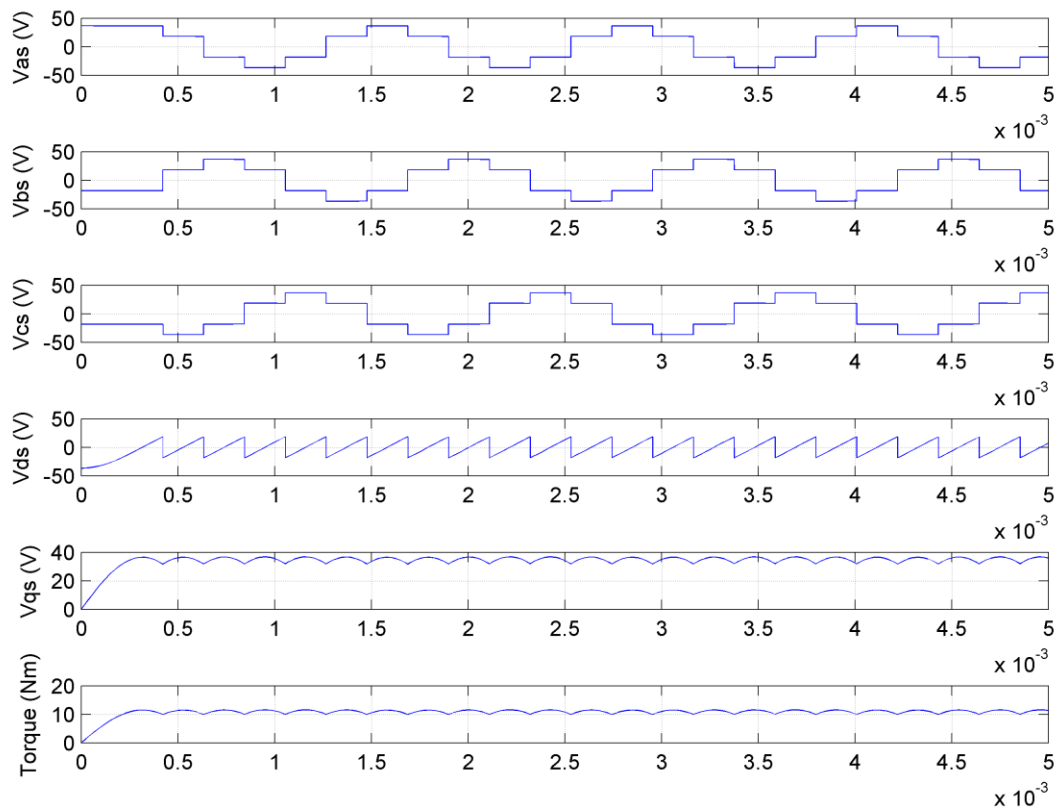


Figure 7.1. Simulation results for the inverter

The pressure in the accumulator was calculated for different values of angular speed in the shaft of the hydraulic pump. These simulations were made for constant speed. The results for the pressure in the hydraulic accumulator are presented in figure 7.2.

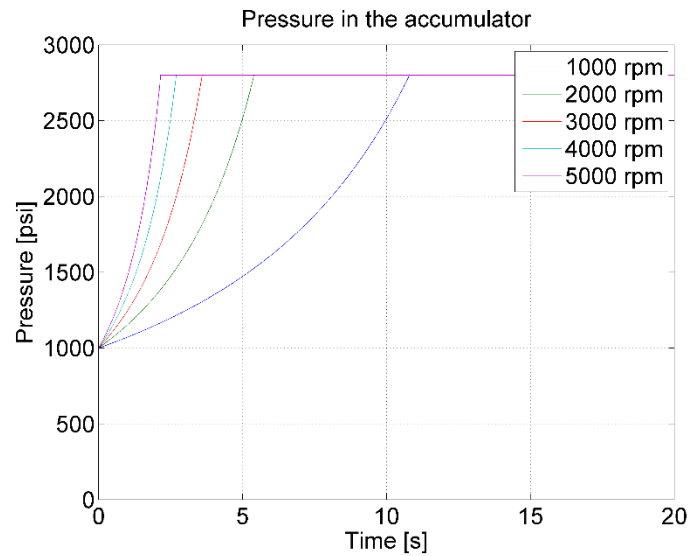


Figure 7.2. Pressure in the accumulator for different operating conditions.

The power in the hydraulic pump is presented in figure 7.3.

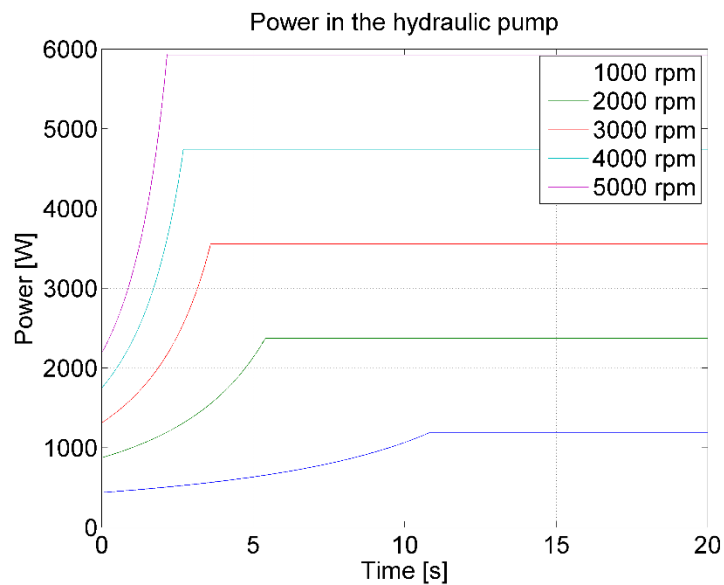


Figure 7.3. Power in the hydraulic pump for different operating conditions.

The current coming from the battery was obtained with the numerical model. The current of the battery is presented in figure 7.4.

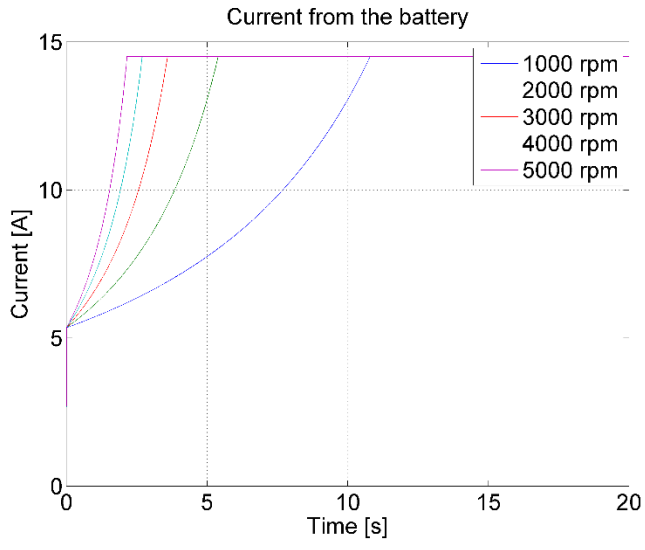


Figure 7.4. Current for the battery.

The results for the model of the electric generator are presented in figure 7.5. A comparison between a desired value of pressure and the actual value is presented.

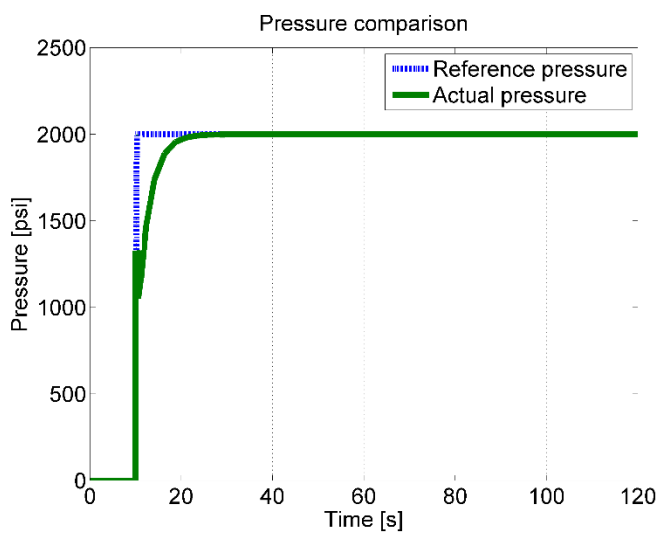


Figure 7.5. Pressure results comparison.

The control signal for the electric generator is presented in figure 7.6.

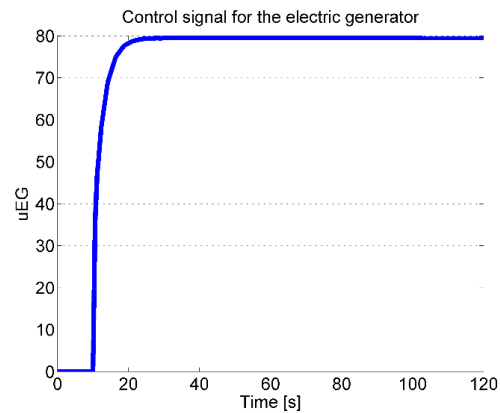


Figure 7.6. Control signal for the electric generator.

7.2 Testbench Results

The main purpose of the testbench is to follow driving schedules and simulate different load conditions for an electrohydraulic system. It is possible to change the load in the system by activating the rheostats which are used to dissipate the power. A test with a variable load was done to study the performance of the system. The number of rheostats was gradually increased. The results for the pressure in the system, the flow rate, and the angular speed in the hydraulic pump and motor are shown in figure 7.7.

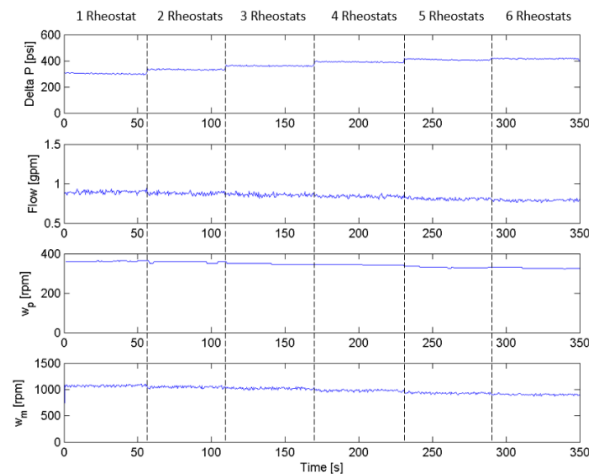


Figure 7.7. Hydraulic variables in the system as the load changes.

A similar test was done, but this time the load was change by activating either one or six rheostats. The results are presented in figure 7.8.

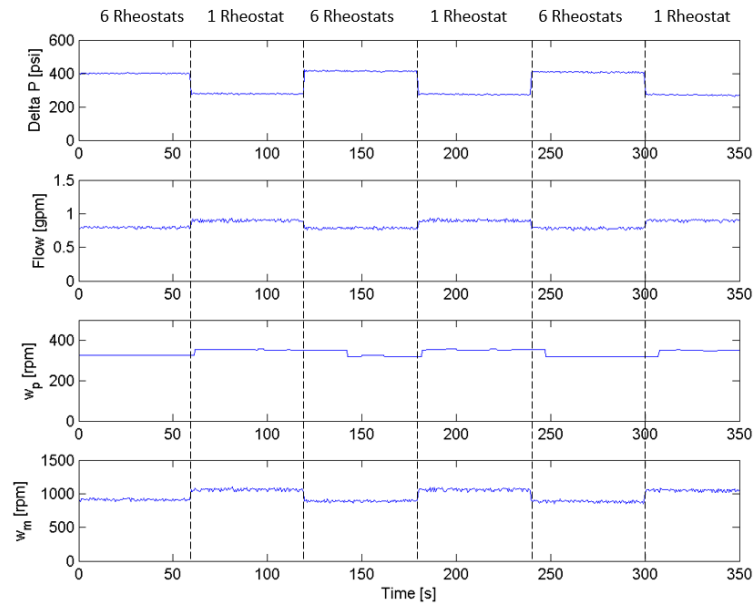


Figure 7.8. Hydraulic variables in the system as the load changes with one or six rheostats.

The power in the system and the efficiency is shown in figure 7.9.

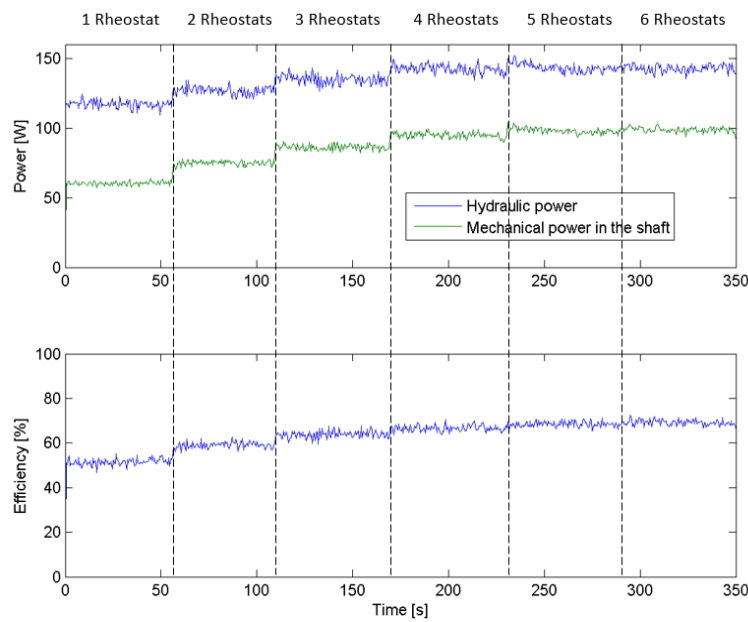


Figure 7.9. Power in the system and efficiency.

The power in the system and the efficiency is shown in figure 7.10 for the test with one and six rheostats.

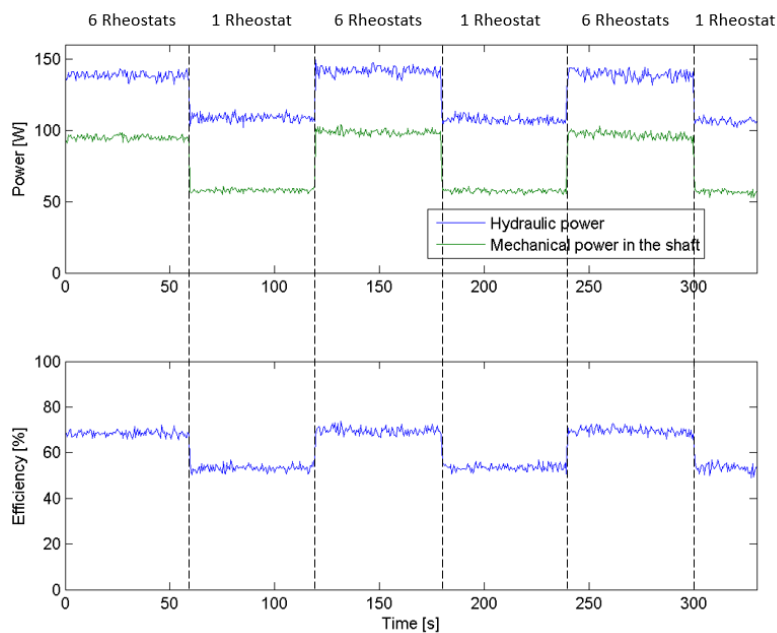


Figure 7.10. Power in the system and efficiency as the load changes with one or six rheostats.

The control algorithm for the shaft speed and the pressure was tested in the testbench. The results are shown in figure 7.11.

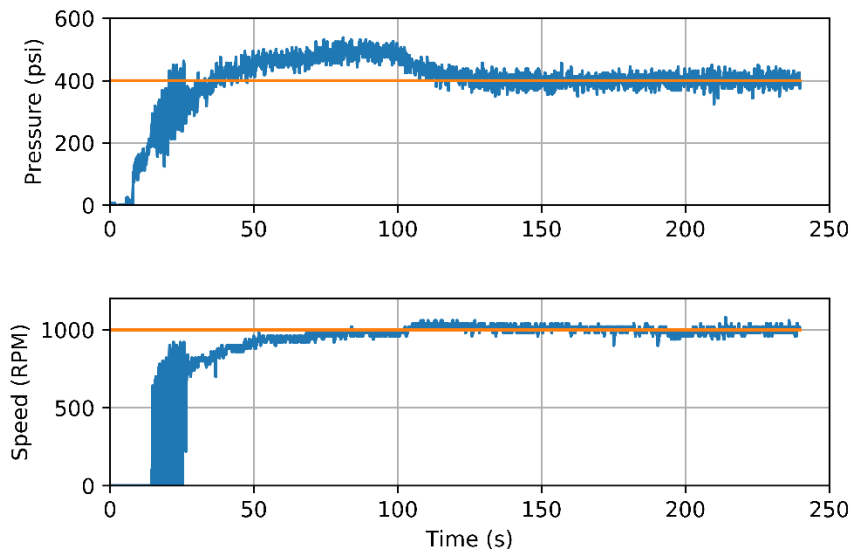


Figure 7.11. Angular speed and pressure in the system.

The control signals for these variables are presented in figure 7.12.

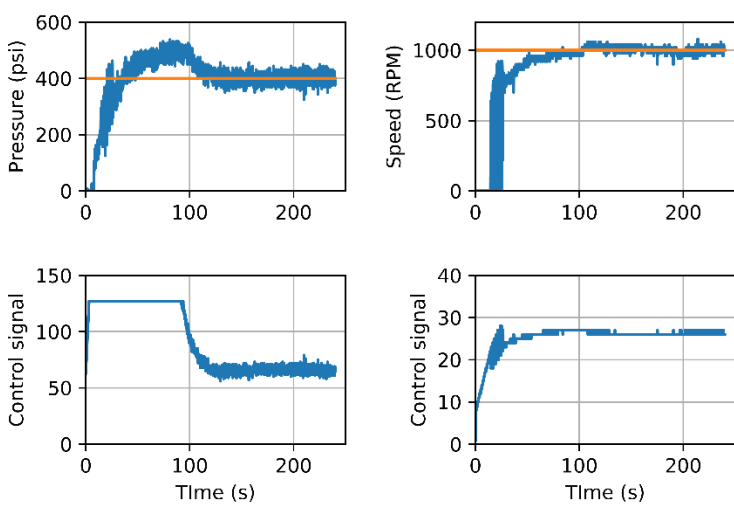


Figure 7.12. Pressure, shaft speed, and control signals in the hydraulic testbench.

The results for different tests with different reference values for the shaft speed are shown in figure 7.13.

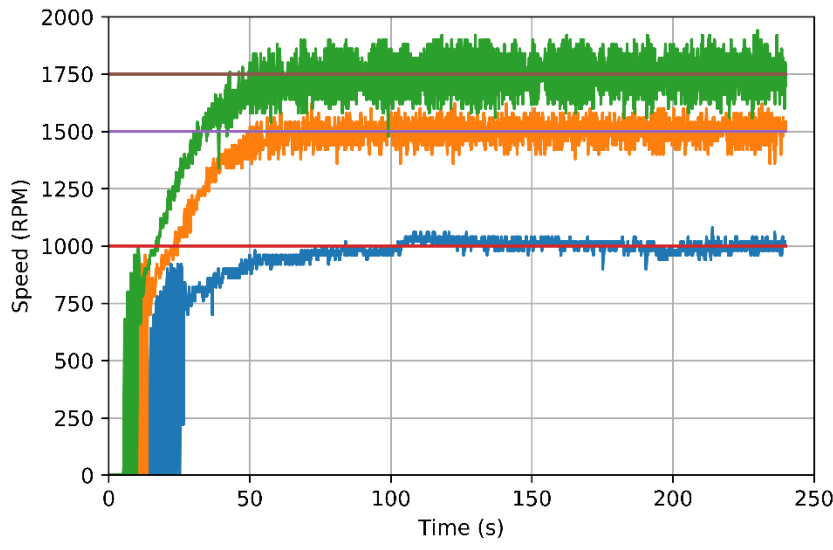


Figure 7.13. Actual speed and reference speed comparison.

The flow rate in the system for these tests is presented in figure 7.14.

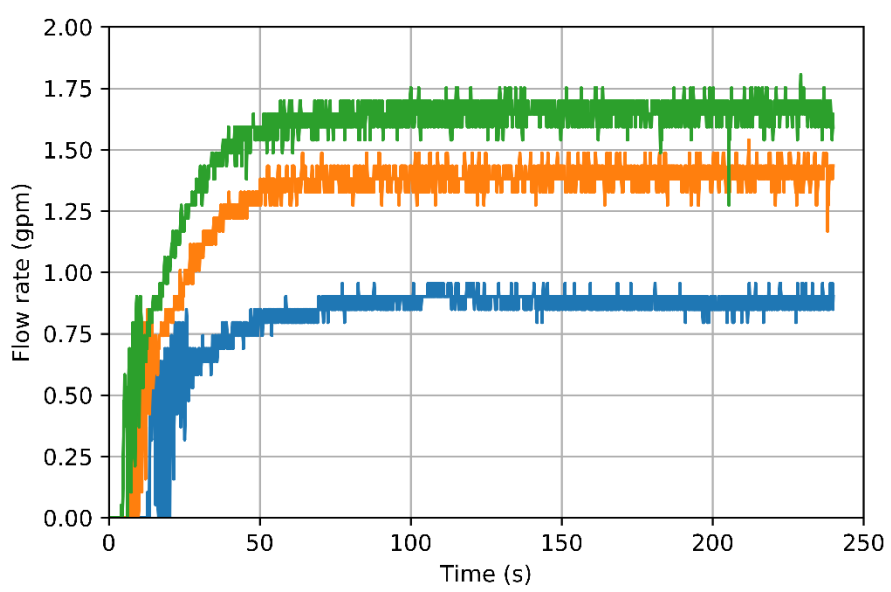


Figure 7.14. Flow rate in the system for different tests.

The control algorithm in the testbench can follow a reference that is changing with the time. The results are shown in figure 7.15.

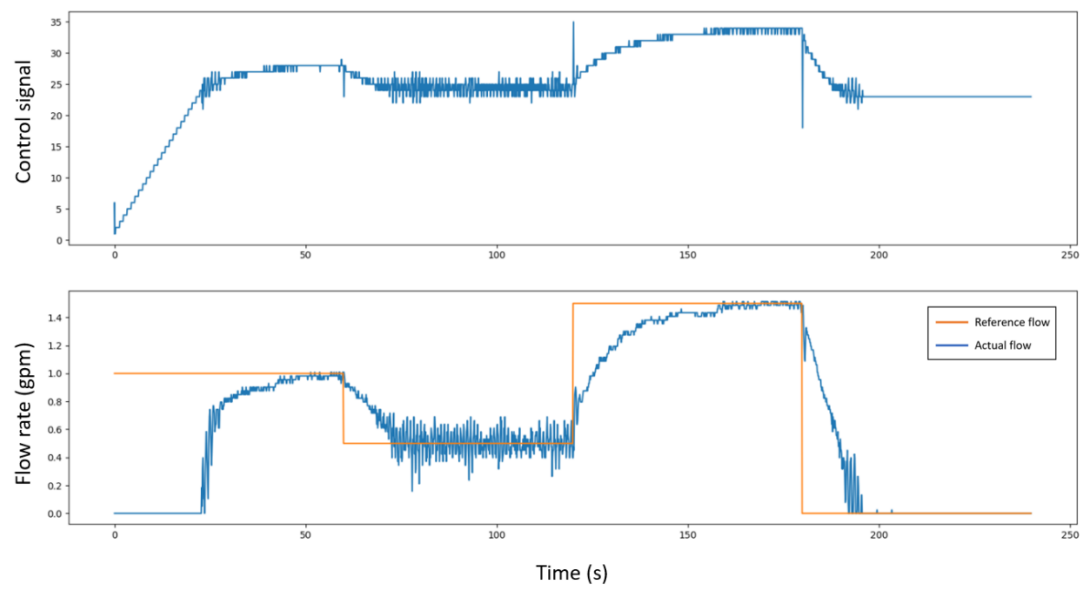


Figure 7.15. Flow rate test for a variable input reference.

The experimental results of the testbench show how the system can be actively controlled for different operating conditions. The operating conditions in the system can be adjusted by changing the number of rheostats connected to the electric generator, and by adjusting the PWM signal that controls the current in the electric generator.

CHAPTER 8. CONCLUSIONS AND FUTURE WORK

The first part of this study, regarding the energy efficiency comparison, has as a result that the hydraulic accumulator has better power/mass, power/volume, and power/cost when compared with a set of ultracapacitors with similar energy storage capacity. The energy efficiency for the ultracapacitor was around 79% and the energy efficiency of the hydraulic accumulator was 87.7%. The power/mass ratio in the set of ultracapacitors was 2.21 kW/kg and 2.69 kW/kg in the hydraulic accumulator. The cost/power ratio is 217 US\$/kW in the ultracapacitors and 75 US\$/kW in the hydraulic accumulator. In terms of energy density, the Energy/mass ratio in the set of ultracapacitors is 2.72 Wh/kg and 0.29 in the hydraulic accumulator. Based on these results, it is possible to conclude that, under the tested conditions, the performance of the hydraulic accumulator is better in terms of power density, but the set of ultracapacitors is better in terms of energy density. Because of that, the hydraulic accumulator was selected as the energy storage system for the testbench designed and constructed. The map of efficiency of the hydraulic accumulator was developed in this part of the study. This map could be used as a tool to establish a control strategy to adjust the pressure and flow in the accumulator to be around the maximum efficiency zone.

The numerical model of the testbench was implemented. This numerical model was divided into three categories: the prime mover model, the hydraulic system model, and the load simulator model. The results for the prime mover model show how the inverter converts the dc voltage from the battery into ac voltage for the electric motor. It is possible to see how the voltage in each phase is shifted with a phase angle, which was the expected result. Also, the results obtained for the voltage in the rotor-frame variables are typical, as well as the electric torque. So it is possible to conclude that this model can be adjusted to simulate different operating conditions for the inverter and the prime mover.

The second part of the numerical modeling of the testbench is the model of the hydraulic devices. The pressure in the hydraulic accumulator was modeled for different operating conditions. It is possible to see how the pressure in the hydraulic accumulator changes rapidly as the fluid goes into the device. For a speed of 1000 rpm in the hydraulic pump shaft, the charging process takes

around 11 seconds, and for a speed of 5000 rpm the charging process takes around 2.4 seconds. According to the simulation results, the power needed to charge the accumulator in 10 seconds is around 1100 W and to charge the accumulator in 2.4 seconds the power needed is around 6000 W. The current from the battery is shown as a result of the simulations. The maximum current output in the battery is 14 Amps, and it is the same for all the speed values tested because the current is coupled with the load in the system. The accumulator was charged until its pressure reaches a maximum value of 2800 psi, this maximum value was the same for all the speed values tested, so that is why the maximum current is the same.

The last part of the numerical model is the load simulator model, which is a model of the electric generator attached to the hydraulic motor shaft. This model was created by modeling the electric machine as a dc generator. The mechanical and electrical behavior is coupled in this system, and the mechanical characteristics of the systems depends on the pressure. A transfer function that relates the pressure in the system and the control signal in the electric generator was defined. The values for the electric constants were defined with experimental results. The control algorithm of this electric generator was simulated, and it is possible to see how the actual pressure in the system follows the reference value. The control signal in the system changes from 0 to 80, so as high is the control signal, as high is the pressure in the system and the load. The maximum value of this control signal could be 128, which is the value given by the digital potentiometer that is used as the input of this controller in the real hardware application.

The experimental results of the testbench show how system can be actively controlled for different operating conditions. The operating conditions in the system can be adjusted by changing the number of rheostats connected to the electric generator. Different variables in the system were measured such as the angular shaft speed in the hydraulic pump, the hydraulic motor, the pressure in the system, and the flow rate. It is possible to see that the pressure in the system increases when the number of rheostats connected increases. This happens because when the number of rheostats increases, the current in the system increases and the pressure increases as well, it is like having a brake attached to the shaft of the system. The power in the hydraulic system and the power in the mechanical system was calculated as well. The efficiency of the system is presented in the result section, it is possible to see that the efficiency increases gradually as the number of rheostats

increases, but the difference in efficiency is not very high when five or six rheostats are connected. These results show that the load and the power dissipated in the system can be controlled and changed in the testbench.

The next step in the experimental tests was the implementation of the control algorithm in the real testbench using hardware. The control algorithm was successfully implemented, the results for the pressure in the system and the angular speed in the electric generator show how the control system can follow a desired reference value. Two different controllers were implemented: one controller for the pressure in the system, and one controller for the speed. Even though the two controllers were programmed and installed independently from each other, they work at the same time in a coupled way. From the results of the control signals, it is possible to see that the controller of the speed can resemble the behavior of an accelerator pedal, because when the control signal increases, the speed increases as well. On the other hand, the control signal for the pressure controller begins with the maximum value because the pressure at the beginning of the test is zero. When the pressure is greater than the reference value, the control signal decreases in order to make the pressure to go down until it reaches the desired value. Different tests were performed for different reference values for the speed. The results show how the hydraulic system can track the desired input reference. The final test is done by changing the reference value, and it is possible to see how the system can follow the reference.

REFERENCES

- Ahmadkhanlou, F., & Goodarzi, A. (2011). Hybrid Lithium-ion/Ultracap energy storage systems for plug-in hybrid electric vehicles. *2011 IEEE Vehicle Power and Propulsion Conference*, 1–7. <https://doi.org/10.1109/VPPC.2011.6043196>
- Alegre, S., Míguez, J. V., & Carpio, J. (2017). Modelling of electric and parallel-hybrid electric vehicle using Matlab/Simulink environment and planning of charging stations through a geographic information system and genetic algorithms. *Renewable and Sustainable Energy Reviews*, *74*, 1020–1027. <https://doi.org/10.1016/j.rser.2017.03.041>
- Allagui, A., Freeborn, T. J., Elwakil, A. S., & Maundy, B. J. (2016). Reevaluation of Performance of Electric Double-layer Capacitors from Constant-current Charge/Discharge and Cyclic Voltammetry. *Scientific Reports*, *6*, 38568. <https://doi.org/10.1038/srep38568>
- Andruch, J., & Lumkes, J. H. (2009, October 6). *Regenerative Hydraulic Topographies using High Speed Valves*. <https://doi.org/10.4271/2009-01-2847>
- Baumann, B. M. (1997). *Intelligent control strategies for hybrid vehicles using neural networks and fuzzy logic* [Master Thesis]. Ohio State University.
- Baumann, B. M., Washington, G., Glenn, B. C., & Rizzoni, G. (2000). Mechatronic design and control of hybrid electric vehicles. *IEEE/ASME Transactions on Mechatronics*, *5*(1), 58–72. <https://doi.org/10.1109/3516.828590>
- Beaman, B. G., & Rao, G. M. (1998). Hybrid battery and flywheel energy storage system for LEO spacecraft. *Thirteenth Annual Battery Conference on Applications and Advances. Proceedings of the Conference*, 113–116. <https://doi.org/10.1109/BCAA.1998.653851>
- Bender, F. A., Bosse, T., & Sawodny, O. (2014). An investigation on the fuel savings potential of hybrid hydraulic refuse collection vehicles. *Waste Management*, *34*(9), 1577–1583. <https://doi.org/10.1016/j.wasman.2014.05.022>
- Bleazard, T., Haria, H., Sprengel, M., & Ivantysynova, M. (2015). *Optimal Control and Performance Based Design of the Blended Hydraulic Hybrid*. V001T01A027. <https://doi.org/10.1115/FPMC2015-9543>
- Boretti, A. (2017). Numerical Study of the Operation of Motorcycles Covering the Urban Dynamometer Driving Schedule. *Advances in Technology Innovation*, *2*(4), 105–112.

- Bozic, A. (2007). *Introducing Hydraulic-Electric Synergy into Hybrid Transmission Using the Free-piston Engine Technology* (SAE Technical Paper No. 2007-01-4112). SAE International. <https://doi.org/10.4271/2007-01-4112>
- Buchwald, P., Christensen, G., Larsen, H., & Pedersen, P. S. (1979). *Improvement of Citybus Fuel Economy Using a Hydraulic Hybrid Propulsion System—A Theoretical and Experimental Study* (SAE Technical Paper No. 790305). SAE International. <https://doi.org/10.4271/790305>
- Çağatay Bayindir, K., Gözükcük, M. A., & Teke, A. (2011). A comprehensive overview of hybrid electric vehicle: Powertrain configurations, powertrain control techniques and electronic control units. *Energy Conversion and Management*, 52(2), 1305–1313. <https://doi.org/10.1016/j.enconman.2010.09.028>
- Cao, J., & Emadi, A. (2012). A New Battery/UltraCapacitor Hybrid Energy Storage System for Electric, Hybrid, and Plug-In Hybrid Electric Vehicles. *IEEE Transactions on Power Electronics*, 27(1), 122–132. <https://doi.org/10.1109/TPEL.2011.2151206>
- Cheng, Y. (2010). Assessments of Energy Capacity and Energy Losses of Supercapacitors in Fast Charging–Discharging Cycles. *IEEE Transactions on Energy Conversion*, 25(1), 253–261. <https://doi.org/10.1109/TEC.2009.2032619>
- Chrostowski, H., & Kędzia, K. (2005). *The analysis of pneumo-hydraulic accumulator efficiency, applied as element of hybrid driving system*. <https://dk.upce.cz/handle/10195/32094>
- Dorey, R. E. (1988). Modeling of losses in pumps and motors. *Proceeding of the First Bath International Fluid Workshop*, 71–97.
- Duran, A., & Walkowicz, K. (2013). A Statistical Characterization of School Bus Drive Cycles Collected via Onboard Logging Systems. *SAE International Journal of Commercial Vehicles*, 400–406.
- Egbue, O., & Long, S. (2012). Barriers to widespread adoption of electric vehicles: An analysis of consumer attitudes and perceptions. *Energy Policy*, 48, 717–729. <https://doi.org/10.1016/j.enpol.2012.06.009>
- Ehsani, M. (2018). *Modern electric, hybrid electric, and fuel cell vehicles* (Third edition..).

- Fouda, M. E., Elwakil, A. S., Radwan, A. G., & Allagui, A. (2016). Power and energy analysis of fractional-order electrical energy storage devices. *Energy*, *111*, 785–792.
<https://doi.org/10.1016/j.energy.2016.05.104>
- Franke, T., & Krems, J. F. (2013). What drives range preferences in electric vehicle users? *Transport Policy*, *30*, 56–62. <https://doi.org/10.1016/j.tranpol.2013.07.005>
- Franke, T., Neumann, I., Bühler, F., Cocron, P., & Krems, J. F. (2012). Experiencing Range in an Electric Vehicle: Understanding Psychological Barriers. *Applied Psychology*, *61*(3), 368–391. <https://doi.org/10.1111/j.1464-0597.2011.00474.x>
- Freeborn, T. J. (2016). Estimating supercapacitor performance for embedded applications using fractional-order models. *Electronics Letters*, *52*(17), 1478–1480.
<https://doi.org/10.1049/el.2016.1740>
- Gillespie, T. (1992). *Fundamentals of Vehicle Dynamics*. SAE International.
- Hartley, T. T., Veillette, R. J., Adams, J. L., & Lorenzo, C. F. (2015). Energy storage and loss in fractional-order circuit elements. *IET Circuits, Devices Systems*, *9*(3), 227–235.
<https://doi.org/10.1049/iet-cds.2014.0132>
- Hewko, L. O., & Weber, T. R. (1990). Hydraulic Energy Storage Based Hybrid Propulsion System For A Terrestrial Vehicle. *Proceedings of the 25th Intersociety Energy Conversion Engineering Conference*, *4*, 99–105.
<https://doi.org/10.1109/IECEC.1990.716464>
- Hibi, A., & Ichikawa, T. (1976). Torque performance of pressure balanced type vane motor at start and in low speed range. *Bulletin of the JSME*, *19*(138).
- Holland, M. A. (2012). *Design of digital pump/motors and experimental validation of operating strategies* [Ph.D.].
<http://search.proquest.com/docview/1220882477/abstract/E7035719CE7F41E0PQ/1>
- Hu, H. (2012). *Advanced hybrid powertrains for commercial vehicles*. Society of Automotive Engineers.
- Hui, S., Lifu, Y., Junqing, J., & Yanling, L. (2011). Control strategy of hydraulic/electric synergy system in heavy hybrid vehicles. *52*, 668–674.
- Hui, Sun, Lifu, Y., & Junqing, J. (2010). Hydraulic/electric synergy system (HESS) design for heavy hybrid vehicles. *Energy*, *35*(12), 5328–5335.
<https://doi.org/10.1016/j.energy.2010.07.027>

- Huria, T., Ceraolo, M., Gazzarri, J., & Jackey, R. (2012). High fidelity electrical model with thermal dependence for characterization and simulation of high power lithium battery cells. *2012 IEEE International Electric Vehicle Conference*, 1–8.
<https://doi.org/10.1109/IEVC.2012.6183271>
- Hyeoun-Dong Lee, Euh-Suh Koo, Seung-Ki Sul, Joohn-Sheok Kim, Kamiya, M., Ikeda, H., Shinohara, S., & Yoshida, H. (2000). Torque control strategy for a parallel-hybrid vehicle using fuzzy logic. *IEEE Industry Applications Magazine*, 6(6), 33–38.
<https://doi.org/10.1109/2943.877838>
- Inaguma, Y., & Hibi, A. (2005). Vane pump theory for mechanical efficiency. *Journal of Mechanical Engineering Science*, 219.
- Itani, K., Bernardinis, A. D., Khatir, Z., Jammal, A., & Oueidat, M. (2016). Regenerative Braking Modeling, Control, and Simulation of a Hybrid Energy Storage System for an Electric Vehicle in Extreme Conditions. *IEEE Transactions on Transportation Electrification*, 2(4), 465–479. <https://doi.org/10.1109/TTE.2016.2608763>
- Jalil, N., & Kheir, N. (1998). *Energy Management Studies for a New Generation of Vehicles (Milestone No.5: Fuzzy logic for the series hybrid)*.
- Jiang, X., Zhang, J., & Jian, W. (2013). The Analysis of Ultracapacitor Charging Efficiency. *2013 International Conference on Computational and Information Sciences*, 1198–1201.
<https://doi.org/10.1109/ICCIS.2013.317>
- Jing, W. X., Zhen, L. M., Wei, S. Y., & Wang, X. (2018). Research on low-speed performance of continuous rotary electro-hydraulic servo motor based on robust control with Adaboost prediction. *The Journal of Engineering*. <https://doi.org/10.1049/joe.2018.8970>
- Johnson, R., & Manring, N. (1994). Modeling a variable displacement pump. *Proceedings of the 1994 ASME Fluids Engineering Division Summer Meeting*, 1–10.
- Ju, F., Zhang, Q., Deng, W., & Li, J. (2014). Review of structures and control of battery-supercapacitor hybrid energy storage system for electric vehicles. *2014 IEEE International Conference on Automation Science and Engineering (CASE)*, 143–148.
<https://doi.org/10.1109/CoASE.2014.6899318>
- Kauranne, H., Ellman, A., Kajaste, J., & Pietola, M. (2003). Applicability of pump models for varying operational conditions. *Proceedings of IMECE2003*, 45–54.

- K.-E. Rydberg. (2009). *Energy Efficient Hydraulic Hybrid Devices*. 11th Scandinavian International Conference on Fluid Power, SICFP, Linkoping, Sweden.
- Keil, P., & Jossen, A. (2014). Improving the Low-Temperature Performance of Electric Vehicles by Hybrid Energy Storage Systems. *2014 IEEE Vehicle Power and Propulsion Conference (VPPC)*, 1–6. <https://doi.org/10.1109/VPPC.2014.7007087>
- Kepner, R. P. (2002). Hydraulic Power Assist – A Demonstration of Hydraulic Hybrid Vehicle Regenerative Braking in a Road Vehicle Application. *SAE Transactions*, *111*, 826–833. JSTOR.
- Kim, S.-, & Sul, S.-. (2006). Control of Rubber Tyred Gantry Crane With Energy Storage Based on Supercapacitor Bank. *IEEE Transactions on Power Electronics*, *21*(5), 1420–1427. <https://doi.org/10.1109/TPEL.2006.880260>
- Kohmascher, T. (2008). *Modellbildung, Analyse und Auslegung hydrostatischer Antriebsstrangkonzeppte*. Aachen University.
- Kohmascher, T., Murrenhoff, H., Rahmfeld, R., & Skirde, E. (2007). Improved loss modeling of hydrostatic units: Requirement for precise simulation of mobile working machine drivelines. *Proceedings of IMECE2007*. IMECE 2007.
- Kono, H. (1998). *Fuzzy control for hybrid electric vehicles* [Master Thesis]. The Ohio State University.
- Kumar, M. R., Ghosh, S., & Das, S. (2019). Analytical Formulation for Power, Energy, and Efficiency Measurement of Ultracapacitor Using Fractional Calculus. *IEEE Transactions on Instrumentation and Measurement*, 1–11. <https://doi.org/10.1109/TIM.2019.2899479>
- Kwon, T.-S., Lee, S.-W., Sul, S.-K., Park, C.-G., Kim, N.-I., Kang, B., & Hong, M. (2010). Power Control Algorithm for Hybrid Excavator With Supercapacitor. *IEEE Transactions on Industry Applications*, *46*(4), 1447–1455. <https://doi.org/10.1109/TIA.2010.2049815>
- Laser, M., & Lynd, L. R. (2014). Comparative efficiency and driving range of light- and heavy-duty vehicles powered with biomass energy stored in liquid fuels or batteries. *Proceedings of the National Academy of Sciences*, *111*(9), 3360–3364. <https://doi.org/10.1073/pnas.1314039111>
- Leon, J., Garcia, J. M., Acero, M. J., Gonzalez, A., Niu, G., & Krishnamurthy, M. (2016). *Case Study of an Electric-Hydraulic Hybrid Propulsion System for a Heavy Duty Electric*

- Vehicle* (SAE Technical Paper No. 2016-01-8112). SAE International.
<https://doi.org/10.4271/2016-01-8112>
- Leon Quiroga, J. A., Gonzalez Mancera, A. L., & Garcia Bravo, J. M. (2017). *A Fuzzy Logic Controller for a Hydrostatic Transmission for an Electric Hybrid Bus in Bogotá, Colombia*. V001T01A042. <https://doi.org/10.1115/FPMC2017-4284>
- Liang, J., Zhang, J., Zhang, X., Yuan, S., & Yin, C. (2013). Energy management strategy for a parallel hybrid electric vehicle equipped with a battery/ultra-capacitor hybrid energy storage system. *Journal of Zhejiang University SCIENCE A*, 14(8), 535–553.
<https://doi.org/10.1631/jzus.A1300068>
- Lin, T., Zhou, S., Chen, Q., & Fu, S. (2018). A Novel Control Strategy for an Energy Saving Hydraulic System With Near-Zero Overflowing Energy-Loss. *IEEE Access*, 6, 33810–33818. <https://doi.org/10.1109/ACCESS.2018.2834343>
- Lin, Tianliang, Chen, Q., Ren, H., Huang, W., Chen, Q., & Fu, S. (2017). Review of boom potential energy regeneration technology for hydraulic construction machinery. *Renewable and Sustainable Energy Reviews*, 79, 358–371.
<https://doi.org/10.1016/j.rser.2017.05.131>
- Lin, Tianliang, Huang, W., Ren, H., Fu, S., & Liu, Q. (2016). New compound energy regeneration system and control strategy for hybrid hydraulic excavators. *Automation in Construction*, 68, 11–20. <https://doi.org/10.1016/j.autcon.2016.03.016>
- Lin, Tianliang, Wang, Q., Hu, B., & Gong, W. (2010). Development of hybrid powered hydraulic construction machinery. *Automation in Construction*, 19(1), 11–19.
<https://doi.org/10.1016/j.autcon.2009.09.005>
- Liu, T., Jiang, J., & Sun, H. (2009). Investigation to Simulation of Regenerative Braking for Parallel Hydraulic Hybrid Vehicles. *2009 International Conference on Measuring Technology and Mechatronics Automation*, 2, 242–245.
<https://doi.org/10.1109/ICMTMA.2009.418>
- Lukic, S. M., Cao, J., Bansal, R. C., Rodriguez, F., & Emadi, A. (2008). Energy Storage Systems for Automotive Applications. *IEEE Transactions on Industrial Electronics*, 55(6), 2258–2267. <https://doi.org/10.1109/TIE.2008.918390>

- M. Ivantysynova, & M. Sprengel. (2013). *Investigation and Energetic Analysis of a Novel Hydraulic Hybrid Architecture for On-Road Vehicles*. The 13th Scandinavian International Conference on Fluid Power, Linkping, Sweden.
- Matheson, P., & Stecki, J. (2003). *Modeling and Simulation of a Fuzzy Logic Controller for a Hydraulic-Hybrid Powertrain for Use in Heavy Commercial Vehicles* (SAE Technical Paper No. 2003-01-3275). SAE International. <https://doi.org/10.4271/2003-01-3275>
- McCandlish, D., & Dorey, R. E. (1984). The mathematical modeling of hydrostatic pumps and motors. *Proceedings of the Institution of Mechanical Engineers, 198B(10)*, 165–174.
- Merrill, K., Holland, M., Batdorff, M., & Jr, J. L. (2010). Comparative Study of Digital Hydraulics and Digital Electronics. *International Journal of Fluid Power, 11(3)*, 45–51. <https://doi.org/10.1080/14399776.2010.10781014>
- Mike Heskitt, Tim Smith, & Jeff Hopkins. (2016, March 12). *Design & Development of the LCO-140H Series Hydraulic Hybrid Low Floor Transit Bus, FTA Report Number 0018* [Text]. Federal Transit Administration. https://www.transit.dot.gov/sites/fta.dot.gov/files/FTA_Report_No._0018.pdf
- Mikeska, D., & Ivantysynova, M. (2002). A precise steady state model of displacement machines for the application in virtual prototyping of power split drives. *Proceedings of the 2nd PhD Symposium 2002*. 2nd PhD Symposium 2002, Modena, Italy.
- Miller, J., & Mitchell, P. (2011). *Ultracapacitor Applications*. Institution of Engineering & Technology. <http://ebookcentral.proquest.com/lib/purdue/detail.action?docID=827220>
- Minav, T. A., Laurila, L. I. E., Immonen, P. A., Haapala, M. E., & Pyrhonen, J. J. (2009). Electric energy recovery system efficiency in a hydraulic forklift. *IEEE EUROCON 2009*, 758–765. <https://doi.org/10.1109/EURCON.2009.5167719>
- Moayedí, S., Cingöz, F., & Davoudi, A. (2013). Accelerated Simulation of High-Fidelity Models of Supercapacitors Using Waveform Relaxation Techniques. *IEEE Transactions on Power Electronics, 28(11)*, 4903–4909. <https://doi.org/10.1109/TPEL.2013.2250522>
- Murray, D. B., & Hayes, J. G. (2015). Cycle Testing of Supercapacitors for Long-Life Robust Applications. *IEEE Transactions on Power Electronics, 30(5)*, 2505–2516. <https://doi.org/10.1109/TPEL.2014.2373368>
- N. Clark, F. Zhen, W. Wayne, & D. Lyons. (2007). *Transit Bus Life Cycle Cost and Year 2007 Emissions Estimation*.

- Nielson, G., & Emadi, A. (2011). Hybrid energy storage systems for high-performance hybrid electric vehicles. *2011 IEEE Vehicle Power and Propulsion Conference*, 1–6. <https://doi.org/10.1109/VPPC.2011.6043052>
- Niu, G., Shang, F., Krishnamurthy, M., & Garcia, J. M. (2017). Design and Analysis of an Electric Hydraulic Hybrid Powertrain in Electric Vehicles. *IEEE Transactions on Transportation Electrification*, 3(1), 48–57. <https://doi.org/10.1109/TTE.2016.2628792>
- Njabeleke, I. A., Pannett, R. F., Chawdhry, P. K., & Burrows, C. R. (1998). Self-organising fuzzy logic control of a hydrostatic transmission. *UKACC International Conference on Control '98 (Conf. Publ. No. 455)*, 1, 66–72 vol.1. <https://doi.org/10.1049/cp:19980203>
- Ossyra, J.-C., & Ivantysynova, M. (2004, October 26). *Drive Line Control for Off-Road Vehicles Helps to Save Fuel*. <https://doi.org/10.4271/2004-01-2673>
- Ostadi, A., & Kazerani, M. (2015). A Comparative Analysis of Optimal Sizing of Battery-Only, Ultracapacitor-Only, and Battery–Ultracapacitor Hybrid Energy Storage Systems for a City Bus. *IEEE Transactions on Vehicular Technology*, 64(10), 4449–4460. <https://doi.org/10.1109/TVT.2014.2371912>
- Ou, S., Zhou, Y., Lian, J., Jia, P., & Tian, B. (2011). Development of hybrid city bus's driving cycle. *2011 International Conference on Electric Information and Control Engineering*, 2112–2116. <https://doi.org/10.1109/ICEICE.2011.5777149>
- Paladini, V., Donato, T., de Risi, A., & Laforgia, D. (2007). Super-capacitors fuel-cell hybrid electric vehicle optimization and control strategy development. *Energy Conversion and Management*, 48(11), 3001–3008. <https://doi.org/10.1016/j.enconman.2007.07.014>
- Pandey, A., Allos, F., Hu, A. P., & Budgett, D. (2011). Integration of supercapacitors into wirelessly charged biomedical sensors. *2011 6th IEEE Conference on Industrial Electronics and Applications*, 56–61. <https://doi.org/10.1109/ICIEA.2011.5975550>
- Pavel, I., Tudor, B., Hristea, M. A., & Popescu, A.-M. (2017). Maintaining Position of Servo Cylinders by Means of Digital Hydraulics. *Hidraulica; Bucuresti*, 2, 62–67.
- Pearre, N. S., Kempton, W., Guensler, R. L., & Elango, V. V. (2011). Electric vehicles: How much range is required for a day's driving? *Transportation Research Part C: Emerging Technologies*, 19(6), 1171–1184. <https://doi.org/10.1016/j.trc.2010.12.010>

- Pourmovahed, A., Baum, S. A., Fronczak, F. J., & Beachley, N. H. (1988). Experimental evaluation of hydraulic accumulator efficiency with and without elastomeric foam. *Journal of Propulsion and Power*, 4(2), 185–192. <https://doi.org/10.2514/3.23047>
- Rajagopalan, A., Washington, G. N., Rizzoni, G., & Guezennec, Y. (2003). *Development of Fuzzy Logic and Neural Network Control and Advanced Emissions Modeling for Parallel Hybrid Vehicles*. <https://doi.org/10.2172/15006009>
- Rezvani, Z., Jansson, J., & Bodin, J. (2015). Advances in consumer electric vehicle adoption research: A review and research agenda. *Transportation Research Part D: Transport and Environment*, 34, 122–136. <https://doi.org/10.1016/j.trd.2014.10.010>
- Riviera, A. M. (1983). *Hydraulic Accumulator Technology Boosts Transit Bus Fuel Economy* (SAE Technical Paper No. 830648). SAE International. <https://doi.org/10.4271/830648>
- Schlosser, W. M. J. (1961). Mathematical model for displacement pumps and motors. *Hydraulic Power Transmission*, 252–257.
- Schlosser, W. M. J. (1968). The overall efficiency of positive displacement pumps. *BHRA Fluid Power Symposium*, 34–48.
- Schouten, N. J., Salman, M. A., & Kheir, N. A. (2002). Fuzzy logic control for parallel hybrid vehicles. *IEEE Transactions on Control Systems Technology*, 10(3), 460–468. <https://doi.org/10.1109/87.998036>
- Shi, L., & Crow, M. L. (2008). Comparison of ultracapacitor electric circuit models. *2008 IEEE Power and Energy Society General Meeting - Conversion and Delivery of Electrical Energy in the 21st Century*, 1–6. <https://doi.org/10.1109/PES.2008.4596576>
- Sprengel, M., Bleazard, T., Haria, H., & Ivantysynova, M. (2015). Implementation of a Novel Hydraulic Hybrid Powertrain in a Sports Utility Vehicle. *IFAC-PapersOnLine*, 48(15), 187–194. <https://doi.org/10.1016/j.ifacol.2015.10.027>
- Sprengel, M., & Ivantysynova, M. (2014). *Recent Developments in a Novel Blended Hydraulic Hybrid Transmission* (SAE Technical Paper No. 2014-01–2399). SAE International. <https://doi.org/10.4271/2014-01-2399>
- Stienecker, A. W., Stuart, T., & Ashtiani, C. (2006). An ultracapacitor circuit for reducing sulfation in lead acid batteries for Mild Hybrid Electric Vehicles. *Journal of Power Sources*, 156(2), 755–762. <https://doi.org/10.1016/j.jpowsour.2005.06.014>

- Tan, Y., Muttaqi, K. M., Ciufu, P., & Meegahapola, L. (2017). Enhanced Frequency Response Strategy for a PMSG-Based Wind Energy Conversion System Using Ultracapacitor in Remote Area Power Supply Systems. *IEEE Transactions on Industry Applications*, 53(1), 549–558. <https://doi.org/10.1109/TIA.2016.2613074>
- U.S. Energy Information Administration (EIA)—Total Energy Monthly Data. (n.d.). Retrieved June 30, 2019, from <https://www.eia.gov/totalenergy/data/monthly/>
- US EPA, O. (2015, September 16). *Dynamometer Drive Schedules* [Data and Tools]. US EPA. <https://www.epa.gov/vehicle-and-fuel-emissions-testing/dynamometer-drive-schedules>
- Wager, G., McHenry, M. P., Whale, J., & Bräunl, T. (2014). Testing energy efficiency and driving range of electric vehicles in relation to gear selection. *Renewable Energy*, 62, 303–312. <https://doi.org/10.1016/j.renene.2013.07.029>
- Wang, B. (2014). High Speed On-Off Valve Self-adapting Clamping System. *Journal of Applied Sciences*, 14, 279–284. <https://doi.org/10.3923/jas.2014.279.284>
- Wang, C., Yijun, W., & Jiajie, O. (2011). Simulation of fuzzy control strategy for parallel hybrid electric vehicle. *2011 International Conference on Electric Information and Control Engineering*, 2592–2594. <https://doi.org/10.1109/ICEICE.2011.5776961>
- Wang, F. (2011). Comparison between Hydraulic Hybrid and Electric Hybrid Passenger Vehicles using ADVISOR 2004. *In Proc. 52nd National Conference on Fluid Power, 2011*, 31–40.
- Wang, T., Wang, Q., & Lin, T. (n.d.). Improvement of boom control performance for hybrid hydraulic excavator with potential energy recovery—ScienceDirect. *Automation in Construction*, 30, 161–169.
- Wiens, T., & Bitner, D. (2016). *An Efficient, High Performance and Low-Cost Energy Recovering Hydrostatic Linear Actuator Concept*. V001T01A038. <https://doi.org/10.1115/FPMC2016-1775>
- Wilson, W. E. (1946). Rotary-pump theory. *ASME Transactions*, 68, 371–384.
- Wu, B., Lin, C.-C., Filipi, Z., Peng, H., & Assanis, D. (2004). Optimal Power Management for a Hydraulic Hybrid Delivery Truck. *Vehicle System Dynamics*, 42(1–2), 23–40. <https://doi.org/10.1080/00423110412331291562>

- Wu, Z. W., Zhang, Z. L., Yin, C. L., & Zhao, Z. (2012). Design of a soft switching bidirectional DC-DC power converter for ultracapacitor-battery interfaces. *International Journal of Automotive Technology*, 13(2), 325–336. <https://doi.org/10.1007/s12239-012-0030-7>
- Xiao, Q., Wang, Q., & Zhang, Y. (2018). Control strategies of power system in hybrid hydraulic excavator—ScienceDirect. *Automation in Construction*, 17(4), 361–367.
- Yoo, H., Sul, S. K., Park, Y., & Jeong, J. (2008). System Integration and Power-Flow Management for a Series Hybrid Electric Vehicle Using Supercapacitors and Batteries. *IEEE Transactions on Industry Applications*, 44(1), 108–114. <https://doi.org/10.1109/TIA.2007.912749>
- Zarotti, G. L. (1981). Pump efficiencies approximation and modeling. *BHRA Fluid Power Symposium*, 145–164.
- Zhang, J., Lv, C., Gou, J., & Kong, D. (2012). Cooperative control of regenerative braking and hydraulic braking of an electrified passenger car. *Proceedings of the Institution of Mechanical Engineers, Part D: Journal of Automobile Engineering*, 226(10), 1289–1302. <https://doi.org/10.1177/0954407012441884>
- Zhang, X., & Mi, C. (2011). *Vehicle Power Management: Modeling, Control and Optimization*. Springer-Verlag. [//www.springer.com/gp/book/9780857297358](http://www.springer.com/gp/book/9780857297358)
- Zhuge, K., & Kazerani, M. (2014). Development of a hybrid energy storage system (HESS) for electric and hybrid electric vehicles. *2014 IEEE Transportation Electrification Conference and Expo (ITEC)*, 1–5. <https://doi.org/10.1109/ITEC.2014.6861868>